Modeling H_2S Dispersion from San Jacinto-Tizate Geothermal Power Plant, Nicaragua

Mariela A. Aráuz Torres

Faculty of Earth Sciences
University of Iceland
2014

Modeling H_2S Dispersion from San Jacinto-Tizate Geothermal Power Plant, Nicaragua

Mariela A. Aráuz Torres

60 ECTS thesis submitted in partial fulfillment of a
Magister Scientiarum degree in Environment and Natural Resources

Advisors
Dr. Throstur Thorsteinsson
Dr. Thráinn Fridriksson

Examiner
Thorsteinn Jóhannsson

Faculty of Earth Sciences
School of Engineering and Natural Sciences
University of Iceland
Reykjavik, June 2014

Modeling H_2S Dispersion from San Jacinto-Tizate Geothermal Power Plant, Nicaragua
Modeling H_2S Dispersion in San Jacinto-Tizate
60 ECTS thesis submitted in partial fulfillment of a *Magister Scientiarum* degree in Environment and Natural Resources

Faculty of Earth Sciences
School of Engineering and Natural Sciences
University of Iceland
Askja, Sturlugötu 7
107, Reykjavik
Iceland

Telephone: 525 4000

Bibliographic information:
Mariela Aráuz Torres, 2014, *Modeling H_2S Dispersion from San Jacinto-Tizate Geothermal Power Plant, Nicaragua*, Master's thesis, Faculty of Earth Sciences, University of Iceland, pp. 72.

Printing: Háskólaprent
Reykjavik, Iceland, June 2014

Abstract

One of the main environmental concerns during the operation of geothermal power plants is related to hydrogen sulfide emissions (H_2S), which negatively affect the air quality in its environs. National ambient air guidelines for H_2S have not been developed in Nicaragua; hence, project developers voluntarily follow international guidelines for atmospheric emissions and occupational safety. Solution-mineral equilibria considerations and assumed steam consumption by the 72 MW geothermal power plant in San Jacinto-Tizate were used to constrain the annual H_2S emission at 1436.2 tons/year. Dispersion modeling of the H_2S emission from the power plant was carried out using AERMOD model to predict H_2S ground level concentrations in the vicinity of the project. The prevailing spatial distribution of the plume was identified in the W direction of the power plant, spreading towards WNW and WSW. The modeling results show that the operation of the San Jacinto-Tizate geothermal power plant does not have significant impact on air quality of the neighboring communities, since populated places are located outside of the predominant plume pathway during the modeled period January-December 2012. A comparison of the model predictions with averaged measured concentrations in the area showed an underestimation of the measured values in most of the monitoring points, suggesting that the model predictions should be considered indicative rather than accurate. Different sources of discrepancy were identified, namely the source input data used for modeling, the characteristics of the location of the control points, the operation conditions of the power plant when the measurements are done as well as the influence of natural sources of H_2S in the reported measured concentrations The results, however, provide useful information to analyze the spatial distribution and the extents of the plume during a given period, and can assist policy makers and project developer to review and improve the air quality monitoring plans.

To my parents…

.. for showing me that everything is possible through work and effort,

for helping me live my dream to be this strong woman!

To my brothers and sisters…

..for their unconditional support and help to stamp my feet on the ground!

Table of Contents

List of Figures

List of Tables

Acronyms

ACGIH	American Conference of Governmental Industrial Hygienists
CNDC	National Load Dispatch Center
EC	European Commission
EIA	Environmental Impact Assessment
H_2S	Hydrogen Sulfide
IDB	Inter-American Development Bank
INE	Nicaraguan Energy Institute
INETER	Nicaraguan Institute of Territorial Studies
MARENA	Ministry of Environment and Natural Resources
MEM	Ministry of Energy and Mines
MINSA	Ministry of Health
NCG	Non Condensable Gases
OSHA	Occupational Safety and Health Administration
PENSA	Polaris Energy Nicaragua S.A.
PPA	Power Purchase Agreement
SJT	San Jacinto-Tizate
USEPA	U.S. Environmental Protection Agency
WHO	World Health Organization

Acknowledgements

I would like to express my sincere gratitude to the Government of Iceland and the United Nations University Geothermal Training Programme, for giving me the opportunity to undertake Masters Studies at the University of Iceland. I am grateful to the staff of the UNU-GTP and ISOR for their extraordinary kindness and ever present help.

Sincere thanks to my advisors, Dr. Thráinn Fridriksson and Dr. Throstur Thorsteinsson their willingness to take part in this project. Thank you very much for your time, discussions, valuable comments and excellent guidance in the completion of this work.

Further appreciation goes to my employer; the Ministry of Energy and Mines of Nicaragua, for allowing me to participate in this program. I am grateful to my colleagues in the Environmental Management Unit. Special thanks to Mr. Luis Molina and Mr. Geovanni Carranza for supporting this project and assistance in data gathering.

PENSA and INETER are also acknowledged for providing meteorological data without which it would not be possible to carry out this project.

I am grateful to the UNU-GTP fellows and friends especially Oscar Cideos and Vincent Kipkirui for their help and discussions on technical matters about geothermal power plants and data processing.

Above all, I would like to thank God for blessing every day of my life and for giving me the strength to complete this project. I also want in a special way to thank my family for their unconditional support and motivation.

1 Introduction

Nicaragua, the largest country in Central America (129,500 km^2) has the greatest potential for developing geothermal resources in the region (Zúñiga, 2003). The first investigation studies in the country began in the fifties; however, utilization of geothermal resources started in 1983 in the Momotombo Geothermal field.

The Geothermal Master Plan of Nicaragua was completed in 2001, estimating the potential of the country as 1,519 MW_e. Since then, geothermal concessions have been awarded to private foreign companies. A special feature of geothermal areas in Nicaragua is that most of these are located within protected areas in Los Maribios Volcanic Range; therefore geothermal development is of special concern in relation to nature conservation.

Despite the geothermal potential in the country, this renewable energy resource has not been widely utilized. The most significant project in the last decade was the commissioning of a 72 MW Power Plant in the San Jacinto-Tizate Geothermal field, in north western Nicaragua.

Polaris Energy Nicaragua S.A. (PENSA), subsidiary of Ram Power Corporation, has the concession rights for the development of a 40 km^2 area in the San Jacinto-Tizate geothermal field. A 10 MW_e power plant with 2x5 MW back pressure units was operated from June 2005 to April 2012. The project expansion works began in 2008 for a new 2x36 MW condensing units power plant. The first 36 MW condensing unit was commissioned on January 2012 and the second unit in December 2012, bringing the installed capacity of the plant to 72 MW_e. To date, full electricity production has not been reached due to lack of steam and PENSA is currently conducting a remediation program to increase the steam resource of the field and to bring the total generation to approximately 59 - 63 MW (Ram Power, 2013).

With the recent change of technology and increased installed capacity of the power plant, concerns about the effect of the H_2S emissions on air quality of the neighboring communities have arisen. The question of whether the concentration of H_2S in the vicinity of the San Jacinto-Tizate geothermal power plant could exceed ambient air standards and occupational safety guidelines when the plant operates at full load is addressed in this study. For this, a Gaussian dispersion model (AERMOD) is used to estimate H_2S ground level concentration at different locations and time periods.

1.1 Statement of Purpose

Electricity generation is considered the dominant industrial source of air emissions and the main driver of climate change. The development and utilization of renewable energy resources is of outmost importance for climate change mitigation and the search of alternatives for meeting the global growing energy needs.

The government of Nicaragua aims to switch from fossil fuel based energy to renewable energy in the next decade. In order provide reliable energy to the national grid, oil imports

saving and reduction of carbon dioxide emissions to the atmosphere, the development of geothermal projects is of great importance in the current energy strategy.

Although geothermal energy is generally considered an environmentally benign energy source, when geothermal areas are developed, pollutants are usually emitted at a higher rate to the environment than before development (Kristmannsdóttir *et al.*, 2000). In geothermal fields in which all waste fluids are reinjected, non-condensable gases (NCG) in steam are the most important discharges from an environmental perspective (Hunt, 2000). The emission of NCG to the atmosphere during the operation of geothermal power plants can negatively affect the air quality in the vicinity of the projects. Among all the NCG emitted, H_2S is of the greatest environmental concern not only because of its noxious smell in low concentrations, but also its toxicity and health impacts at high concentrations (Kristmannsdóttir *et al.*, 2000).

The commissioning of the San Jacinto-Tizate geothermal power plant certainly means a big step for geothermal development in Nicaragua. Nevertheless, the environmental effects of the project operation on air quality need to be further investigated.

National guidelines for H_2S has not been developed in Nicaragua, hence project developers are encouraged to follow international standards, usually the WHO guidelines. Villages located near the San Jacinto-Tizate project may be exposed to H_2S ambient air concentrations due to emissions from the power plant; however this has not been yet studied in relation to the extent and relevance of the impacts. To date, the only background data on air quality in the area consist of reports prepared by the project developer PENSA, based on limited air quality monitoring carried out at the project site twice a year since 2006.

Dispersion software based on Gaussian plume equation has been widely applied to estimate the diffusion of various air pollutants (Seangkiatiyuth *et al.*, 2011; Thorsteinsson *et al.*, 2013). The present study denotes the first attempt to assess the temporal and spatial distribution of H_2S emissions from the San Jacinto-Tizate power plant using a dispersion model. It is anticipated that the results of this study could assist regulatory bodies and stakeholders in the review and improvement of the air quality monitoring plans as well as the management of the project's environmental effects.

1.2 Objectives

The present study aims to assess the temporal and spatial distribution of H_2S in the surrounds of San Jacinto-Tizate geothermal power station using dispersion modeling. In order to achieve this, the following specific objectives will be met:

- To estimate the H_2S emissions of the 72 MW geothermal power plant.
- To explore the effect of different meteorological parameters on H_2S dispersion in the San Jacinto-Tizate project area.
- To predict H_2S ground level concentrations due to emissions from San Jacinto-Tizate geothermal power plant using AERMOD model.
- To identify areas where high concentration of H_2S could be expected.

- To analyze predicted H_2S ground level concentrations for comparison with international ambient air quality guidelines and occupational safety standards.
- To compare the model predicted H_2S concentrations with measurements during the same period.
- To recommend improvements to the air quality monitoring plan based on the modeling results.

2 Background

2.1 History of Geothermal Development in San Jacinto-Tizate

Exploration studies in the San Jacinto-Tizate geothermal area has been conducted by several institutions and in various successive phases. A summary of the exploration history is given in Table 2-1. The first geoscientific studies in the area were conducted in 1953 and consisted of measurements of heat flow from surface manifestations. Exploration studies conducted from 1969 to 1971 included geological, geochemical and geophysical surveys, and the drilling of shallow temperature gradient wells. Further exploration carried out from 1970-1980, indicated that a high temperature (250 to 300°C) resource existed with a potential resource area of 6 km^2, and a potential considered to be around 100 MW_e.

In late 1992, Intergeoterm S.A., a joint venture between the Nicaraguan electricity company ENEL (77%) and Burgazgeoterm (23%), a subsidiary of Gazprom of Russia, began work on a feasibility study for development of the concession for electricity generation. This work included further surface exploration and the drilling of wells ranging in depth from 728 to 2,339 m. Five of the wells were tested, either by production and/or injection, and three in the Tizate area (SJ4, 5 and 6) were considered to be commercial producers.

In 2001, a concession in the San Jacinto-Tizate geothermal area was awarded to Intergeoterm S.A under an exploitation agreement for a period of 25 years. In 2004 the concession was transferred to San Jacinto Power Company S.A., now Polaris Energy Nicaragua S.A. (subsidiary of Ram Power, Corporation).

Polaris Energy Nicaragua S.A. (PENSA) holds a concession of 40 km^2 in San Jacinto-Tizate area. Electricity production began in 2005 with the commissioning of a 10 MW power plant with 2x5 MW back pressure units. In 2012 a new power plant with 2x36 MW condensing units was commissioned and the backpressure units were taken out of service, bringing the installed capacity of the plant to 72 MW_e. To date, a total of seventeen wells have been drilled in this geothermal field, 7 are production wells (SJ-4, SJ-5, SJ6-2, SJ9-1, SJ9-3, SJ12-2, SJ12-3), 3 reinjection wells (SJ-1, SJ-10 and SJ-11) and one pressure monitoring well (SJ-3). The remaining wells are non-producers or were not completed due to technical problems during drilling.

Table 2-1. Investigation history of the San Jacinto-Tizate geothermal resource (modified from Ogryzlo and Randle, 2005).

Year	Activity
1953	Heat flow measurements by McBirney (McBirney and Williams, 1965)
1969-1971	USAID identified San Jacinto- Tizate area as high priority resource
1970-1980	UNDP delineated potential resource of 6 km^2
1992	DAL SpA (DAL) reviewed previous work and continued survey. Upflow for the field located in the Tizate area with an outflow southward to San Jacinto.
1992	Intergeotherm S.A feasibility study
1993-1995	Drilling of 7 commercial diameter wells
1998-2001	Exploitation concession and power purchase agreement (PPA)
2001-2002	PENSA well testing and feasibility study
2005	Backpressure power plant commissioning
2007-2011	Drilling of new wells and expansion works
2012	Condensing power plant commissioning and backpressure power plant shut down
2013-2014	PENSA remediation program

2.2 Characteristics of the Project Area

San Jacinto-Tizate geothermal field is located in the municipality of Telica, Department of León, Nicaragua. The geothermal concession covers an area of 40 km^2 and it is divided into an eastern section and an undeveloped western section. The estimated geothermal potential of the area is 200 MW. The project site is concentrated in the eastern sector of the concession, encompassing an area of 4 km^2, including the power plant and well platforms, 2.3 km of pipes corridor, access roads (~ 3 km) and a 138 kV transmission line of 12.5 km length (IDB, 2010).

The project site is located approximately 2 km to the north of San Jacinto, a village of approximately 1,400 inhabitants (Figure 2-1). The village is isolated from the project site by low hills. Four settlements dispersed into small dwellings are also found in the eastern sector of the concession area: El Chorro with a population of approximately 245 inhabitants, El Apante Central with 401 inhabitants, La Cruz del Apante with 243 inhabitants and El Ojochal de Liston with 128 inhabitants (IDB, 2010). No indigenous people live in the area and there has been no evidence to date of any archaeological sites finds. Sparse subsistence farming and low-scale non-intensive livestock activity predominates in the area.

The project is located in highly intervened fragmented dry habitat, which is sparsely inhabited, although some subsistence farming activities such as cattle grazing takes place in the eastern sector of the concession. The area does not encompass habitats that could be considered critical or natural, finding a fragmented habitat on the most part of the eastern sector of the concession. No threatened or endangered species have been documented in the project's area (PENSA, 2008).

The geothermal concession overlaps with a protected area; the Volcanic Complex Telica-Rota Nature Reserve, mainly located in the western sector of the concession. The Reserve was created in 1983, covering an area of approximately 9,053 ha, from which 6,846 ha pertain to the Telica Volcano and the remaining area belongs to the Rota Volcano (Figure 2-1). The protected area has been classified within Category IV in the International Union

for Conservation of Nature (IUCN), which management approach is to maintain, conserve and restore species and habitats in areas that have already undergone substantial modification, necessitating protection of remaining fragments, with or without intervention (IUCN, 2012).

The Ministry of the Environment and Natural Resources (MARENA by its Spanish acronym) is in charge of the management of the natural reserve, defining the protected area in the 300 m elevation contour line. In the western sector of the natural reserve, there are small hamlets or isolated farms with an approximate population of 3,800 inhabitants. Similarly to the overall region, the protected area has been highly affected by anthropogenic activities (IDB, 2010).

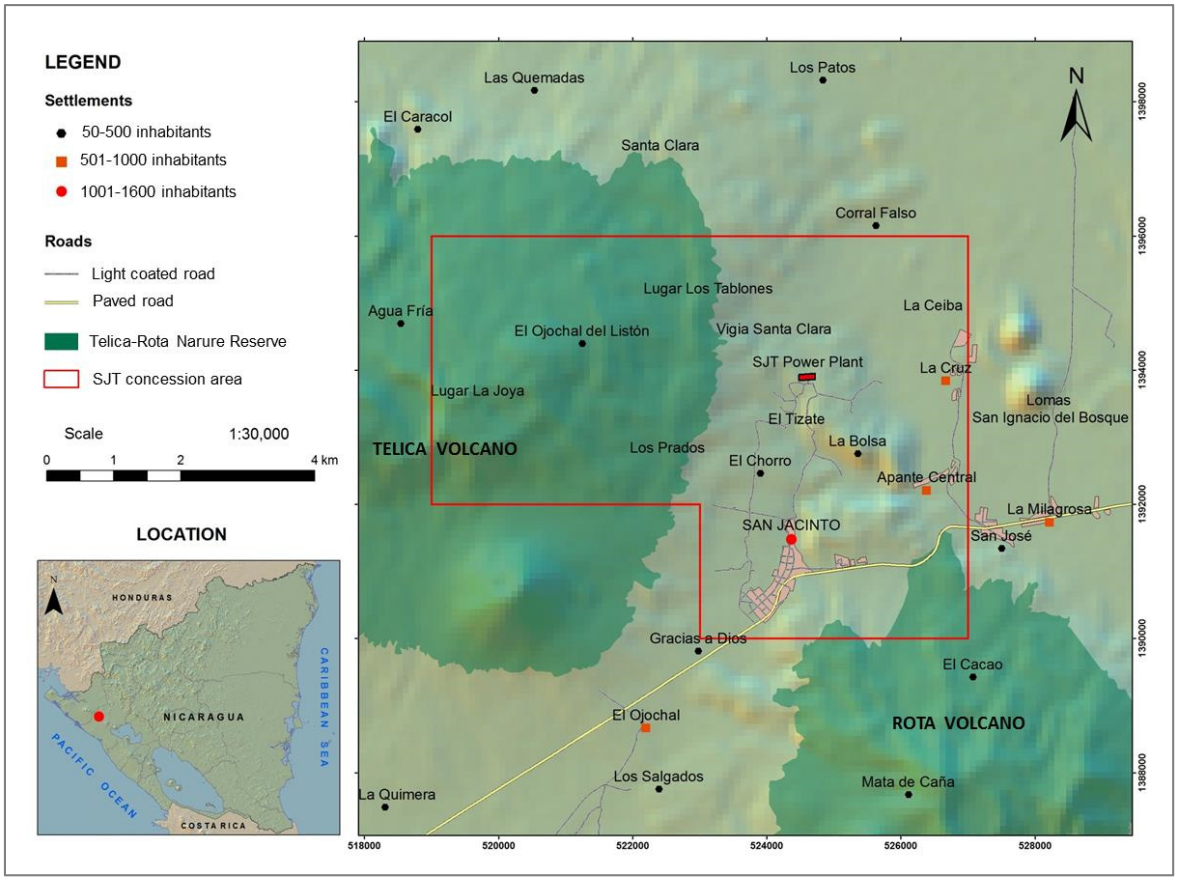

Figure 2-1. Settlements in the San Jacinto-Tizate geothermal concession area (based on IDB, 2010).

A large part of the vegetation in the vicinity of the project area has been extremely modified by agriculture activities, cattle farming and firewood extraction. A substantial part of the area is covered by pasture land. There is an abundance of grazing lands, vast prairies; thin forests with somewhat dense tree patches of 4 to 10 m in height, where *caducifolias* or *subcaducifolias* prevail, and arboreal species are limited to more elevated zones in the volcanic complexes. In addition, in areas with high geothermal activity, the vegetation is scarce due to the soil conditions (high acidity) and high temperature, not prone to development of vegetation (IDB, 2010). Throughout the concession area, natural geothermal manifestations such as fumaroles, mud pools and hot springs are found.

Most of the surface watercourses in the project area have a short path and are intermittent. Both phreatic and artesian aquifers are found in the area as well as hot and cold springs. The chemical composition of water is variable. Analysis performed indicate a calcium bicarbonate composition for springs and calcium bicarbonate and sulfates for freshwater wells in El Tizate area. Natural contamination from geothermal origins is evidenced by abnormal concentrations of mercury, silica and chloride observed. However, the values reported are below the limits recommended by the World Health Organization (WHO) guidelines for drinking water (IDB, 2010). Bored wells or naturally occurring springs represent the main water supply of the rural population in the project area.

2.3 Geothermal Development and Gas Emissions

Geothermal fluids naturally contain various non-condensable gases (gases not easily converted to liquid form via a cooling process); which are also naturally vented to the atmosphere through diffusive gas discharges from areas of natural leakage, including hot springs, fumaroles, geysers, hot pools, and mud pots. These natural discharges have taken place throughout the history of the Earth and continue today independent of geothermal power production. Carbon dioxide is the most widely emitted gas, because geothermal systems tend to be found in areas with large fluxes of carbon dioxide (Holm *et al.*, 2012).

The amount of gases that are present in the geothermal fluid and which might be emitted depends on a variety of factors. The main factors are the resource fluid chemistry, water phase (dry steam or liquid), and temperature, but the type of power plant (back pressure, flash, dry steam, binary, or combined cycle) and the plant characteristics (efficiency and H_2S or other gas abatement systems) also influence emission levels (Bloomfield *et al.*, 2003).

Gas discharges from low-temperature systems do not usually cause significant environmental impacts, however in high-temperature geothermal fields, power generation using a standard steam-cycle plant may result in the release of non-condensable gases (NCG) and fine solid particles into the atmosphere (Webster, 1995). In vapor-dominated fields in which all waste fluids are reinjected, non-condensable gases in steam will be the most important discharges from an environmental perspective (Hunt, 2000).

The concentration of NCG varies not only between fields but can also from well to well within a field, thus changes to the proportion of steam from different wells may cause changes in the amount of NCG discharged. Gas concentrations and composition cover a wide range, but the predominant gases are carbon dioxide (CO_2) and hydrogen sulfide (H_2S). The emissions are mainly from the gas exhausters of the power stations, often discharged through a cooling tower. Gas and particulate discharges during well drilling, bleeding, cleanouts and testing, and from line valves and waste bore water degassing, are usually insignificant (Hunt, 2000).

In liquid dominated geothermal fields, the majority of the gases are dissolved in the fluid in the geothermal system. During utilization and depressurization of the geothermal fluid the gases are concentrated in the steam phase and are finally vented out of the condensers of the turbines to atmosphere (Gunnarsson *et al.*, 2013). The gas emission therefore inevitably affects the air quality around the power plants as the concentration of the geothermal gases increases. Under certain weather conditions and if good distribution of the gases at the

disposal site is not secured, the gases can affect air quality tens of kilometers from the power plant site (Gunnarsson *et al.*, 2013; Thorsteinsson *et al.*, 2013).

The amount of sulfur gases (mainly H_2S) emitted from a geothermal power station (average 0.03 g/kWh) is less than 2% of that emitted from equivalent size coal and oil fired power stations (9.23 and 4.95 g/kWh, respectively). Hydrogen sulfide is contained in most geothermal steam sources and depending on the type of condenser employed the H_2S will partition itself in various ratios between the condensate and the non-condensable gas (NCG). In most populated areas, this H_2S must be removed from the NCG streams prior to exhausting the NCG to atmosphere, and the optimum type of process for removing the H_2S depends on the amount of H_2S in the NCG (Nagl, 1999).

Conventional steam turbine units can be of the back pressure or condensing type. In the back pressure type, the turbine exhaust is simply vented to the atmosphere, which results in an inexpensive but very inefficient operation. The more common condensing turbine is more expensive than a back pressure turbine; however, it is approximately twice as efficient. In condensing units, the mixture of steam and brine from the production wells is flashed and separated. The separated brine is usually reinjected to provide a continual source of fluid for the production of geothermal steam, while the separated steam is directed to the turbine-generator set. The exhaust from the turbines passes through a condenser which produces a condensate stream and a non-condensable gas stream. The NCG can vary from 1% to 20% of the inlet stream to the turbine (Nagl, 1999). In some cases, hydrogen sulfide abatement systems are required, depending on the amount of gas emitted, the characteristics of the geothermal reservoir, the design of the power plant and the local regulatory requirements (Nagl, 1999).

Studies on H_2S emissions to the atmosphere have been made in many geothermal areas around the world. In some countries with extensive geothermal development and utilization, H_2S emissions have posed the utmost environmental concern. The studies have shown that after the development of geothermal areas, the air quality has been negatively affected in nearby towns and villages (e.g. Iceland and New Zealand).

In Iceland, the main environmental concern of high temperature geothermal utilization is the atmospheric disposal of H_2S. Numerous dispersion modeling studies have been conducted for geothermal power plants located in the Hengill area (e.g. Chow-Pineda, 2007; Khoirunissa, 2011; Ólafsdóttir, 2007; Ólafsdóttir *et al.*, 2014; Thorsteinsson *et al.*, 2013). Since commissioning of Hellisheiði Power Plant in 2006 the characteristic smell of H_2S is much more frequent in Reykjavík and the H_2S concentration increased in nearby communities. As a result, a new regulation on atmospheric concentration of H_2S was set by the government of Iceland in 2010 and is due to become valid in July 2014. The new regulation puts high pressure on the geothermal industry in Iceland to lower gas emission from geothermal power plants and more focus was put on H_2S abatement. Currently, experimental projects have been undertaken to develop methods to treat the geothermal gases (Gunnarsson *et al.*, 2013)

Understanding how natural emissions are altered by industrial utilization would require a baseline determination prior to power development, since NCG are present in both producing and non-producing geothermal systems. Such baseline information is usually unavailable in practice unless the area has been the subject of academic research or the measurements have been required for regulatory reasons (Holm *et al.*, 2012).

In the San Jacinto-Tizate geothermal field in Nicaragua, a moderate low gas concentration in the steam has been reported. Ambient air concentration of H_2S in the range of 0.001-0.02 ppm averaged over 24 hours, have been reported in the vicinity of the power plant (PENSA, 2012, 2013). However, studies on the dispersion and spatial distribution of the power plant emissions have not been carried out to date.

2.4 Characteristics of Hydrogen Sulfide

2.4.1 Physical and Chemical Properties

Hydrogen sulfide (H_2S) is a colorless toxic gas characterized by a rotten eggs odor; it is soluble in various liquids including water and alcohol. It can be formed under conditions of deficient oxygen, in the presence of organic material and sulfate (WHO, 2003). A description of the physical and chemical properties is presented in Table 2-2.

Table 2-2. Properties of hydrogen sulfide (AIHA, 1991; WHO, 2000, 2003).

Description	Hydrogen sulfide
Molecular formula	H_2S
Molar mass	34.08 g/mol
Boiling point	-60.4 °C
Melting point	-85.5 °C
Density	1.39 g/l at 25°C
Solubility in water	0.5 g/100 ml at 20°C
Explosive limits	4.3-46 vol% in air
Vapor pressure	1 atm at -60.4°C
Conversion factor	1 ppm = 1.4 mg/m³ at 25°C

2.4.2 Health Effects

Hydrogen sulfide is both an irritant and asphyxiant gas. Levels of up to 20 ppm have generally no effects on healthy people while for asthmatic people this level has to be reduced to 2 ppm (WHO, 2003). Concentrations above 20 ppm may irritate the eyes and respiratory tract, above 50-100 ppm neurotoxic effects appear and 500-1000 ppm are considered of immediate life danger (WHO, 2003). Although the human odor threshold is very low (0.02 ppm), at a concentration of 150 ppm it leads to loss of smell.

H_2S is heavier than air and it can accumulate in closed and/or depressed areas. Some of the fatal incidents with volcanic gases have been attributed to the effect of H_2S released by low temperature fumarolic vents or by gas bubbling through thermal springs (D'Alessandro, 2006).

Health effects depend upon the type and amount of pollutants present, the durations of exposure, and the state of health, age and level of activity of the person exposed (Morris and Therivel, 1995). Although numerous case studies of acute toxic effects of H_2S exist, studies about long-term exposure effects in humans are scarce. The interpretation of most of the studies conducted is very complex because the subject population was in many cases

exposed to other pollutants in addition to H_2S. A brief description of selected studies conducted in areas exposed to both natural and industrial sources of hydrogen sulfide is made below.

A mortality study undertaken among Finnish sulfate mill workers exposed to H_2S and organic sulfides reported an increase in cardiovascular-related deaths compared to national death rates. Cardiovascular mortality was higher in workers employed for 5 years compared to workers exposed for 1-4 years (Jappinen *et al.*, 1990).

The city of Rotorua, New Zealand, is located on an active geothermal field and therefore, is frequently exposed to geothermal gas emissions. Some studies have evidenced health effects from chronic exposure to H_2S (0.1- 2 ppm), strengthening the suggestions that there are chronic health effects from low levels H_2S exposure concerning nervous system diseases and cardiovaculatory diseases (Bates *et al.*, 2002), as well as respiratory diseases (Bates *et al.*, 2002; Durand and Wilson, 2006).

Bates *et al.* (2013) also investigated whether long-term, low-level hydrogen sulfide gas is a cause of asthma in the population of Rotorua city in New Zealand. The study provided no evidence that asthma risk increases with H_2S exposure. Suggestions of reduced risk in the higher exposure areas were consistent with recent evidence that H_2S has signaling functions in the body, including induction of smooth muscle relaxation and reduction of inflammation. However, the authors state some limitations of the study, including possible confounding that preclude definitive conclusions. Another study was recently conducted in the same city by Reed *et al.* (2014). In this, the possible effects on cognitive function in an urban population with chronic, low-level exposure to H_2S were investigated. The results evidenced that chronic H_2S exposure, at the ambient levels found in and around Rotorua, is not associated with impairment of cognitive function.

Kilburn and Warshaw (1995) investigated whether people exposed to sulfide gases, including H_2S demonstrated persistent neurobehavioral dysfunction. The study was conducted on former workers and neighbors of a coastal oil refinery in California, who complained of headaches, nausea, vomiting, depression, personality changes, nosebleeds, and breathing difficulties. Statistically significant neurophysiological abnormalities were associated with exposure to reduced sulfur gases, including H_2S from crude oil desulfurization.

Community residents living near industrial hog operations in eastern North Carolina exhibited acute physical symptoms related to air pollutants comprised mostly of hydrogen sulfide and lower levels of other atmospheric sulfides and amines. Odor and hydrogen sulfide were associated with respiratory symptoms and with eye irritation (Schinasi *et al.*, 2011). Another study in a community bordering a landfill showed a strong association of odor and hydrogen sulfide concentrations with mucosal irritation and upper respiratory symptoms (Heaney *et al.*, 2011).

Carlsen *et al.* (2012) investigated the association between daily ambient levels of hydrogen sulfide, PM_{10}, nitrogen dioxide (NO_2) and ozone (O_3) and the use of drugs for obstructive pulmonary diseases in adults in Iceland's capital area, Reykjavik. Intermittent increases in levels of particle matter from traffic and natural sources and ambient H_2S levels were weakly associated with increased dispensing of drugs for obstructive pulmonary disease,

however, the authors stated that the weak association could be confounded by unevaluated variables and hence further studies are needed.

2.4.3 Environmental Effects

Most of the atmospheric hydrogen sulfide has natural origins, occurring around sulfur springs and lakes, and it is an air contaminant in geothermal areas (WHO, 2000). Volcanic and geothermal areas are one of the major natural sources of H_2S to the atmosphere; however, atmospheric concentrations of H_2S in these areas are generally below toxic levels (D'Alessandro *et al*., 2009).

H_2S is oxidized by photochemical generated free radicals, especially by hydroxyl radicals, forming the sulfhydryl radical and ultimately sulfur dioxide or sulfate compounds (WHO, 2003). The atmospheric residence time of H_2S is typically less than 1 day, but may be as high as 42 days in winter time (WHO, 2003). The resident time varies depending on the presence of photoactive pollutants, temperature, and geographic conditions.

Hydrogen sulfide is unstable in air compared to sulfur dioxide (SO_2) and if conditions are favourable oxidation may take place (Kristmannsdóttir *et al.*, 2000). H_2S dissolved in water aerosols, such as fog, reacts with atmospheric oxygen to form more oxidized sulfur-bearing compounds; some of these compounds have been identified as components of acid rain, but a direct link between H_2S emission and acid rain has not been established (Hunt, 2000).

Several studies about the effect of H_2S on different plant species have been carried out. Thompson and Kats (1978) studied the effects of H_2S and CO_2 from geothermal emission on four important crops: lettuce, sugar beets, cotton and alfalfa. The continuous fumigation of the referred species with 3000 parts per billion (ppb) H_2S in greenhouses caused leaf lesions, defoliation, reduced growth, and death of sensitive species and a concentration of 300 ppb caused lesser but similar effects. Sulfur accumulated in leaves depending upon dosage and fast growing plants accumulated sulfur more rapidly. Lower levels of H_2S, 30 ppb and sometimes 100 ppb, caused significant stimulation in growth of lettuce, sugar beets, and alfalfa. A more recent study also reported H_2S positive effects on plant growth and increased development of plant stress tolerance. Hydrogen sulfide has been identified as a priming agent of seed germination and a photosynthesis enhancement agent (Li, 2013).

Bacci *et al.* (2000) studied the effects of H_2S in vegetation near geothermal power plants in Mt. Amiata (Tuscany, Italy), reporting that sensitive plant species may be affected when exposed to hydrogen sulfide concentrations of 100 $\mu g/m^3$ (70 ppb). Idriss *et al.* (2004) reported no observable effects on vegetation for long-term H_2S exposure at concentrations lower than 140 $\mu g/m^3$ (100 ppb).

2.5 H_2S Ambient Air Guidelines

The ambient air standards are generally health-based guideline values to protect people's health and well-being. Many countries do not have ambient air quality guidelines for H_2S, as it is not perceived as a problem in most regions (IVHHN, 2014). A summary of the WHO guidelines and other ambient air guideline values from countries with extensive geothermal development and utilization is given in Table 2-3.

Table 2-3. H_2S air ambient guidelines in different countries.

Country	Guideline/Regulation	Averaging period	Value ($\mu g/m^3$)
International	WHO Air Quality Guidelines 2nd Edition, 2000	24 hour 30 minutes	150 7
Iceland	H_2S Concentration in the Atmosphere (Regulation No. 514/2010)	24 hour	50 *
New Zealand	Ambient Air Quality Guidelines, 2002	1 hour	7
State of California, USA	CAAQS, State Ambient Air Quality Standards	1 hour	43

* The limit may be exceeded 5 times per year in the effect from the publishing of the regulation (2010). From 1st July 2014, the limit shall not be exceeded.

The WHO Air Quality Guidelines also gives a value for smell to become a nuisance at 7 $\mu g/m^3$ over at 30 minute average. In New Zealand, the guideline value for hydrogen sulfide is based on preventing odor annoyance and the resulting impacts on well-being rather than specific health effects, stipulating that the guideline value may not be suitable for geothermal areas. In the case of Iceland, the limit value for H_2S concentration in the atmosphere was set to prevent harmful effects to the general population and the environment as a whole.

The California Ambient Air Quality Standard for hydrogen sulfide was based on the geometric mean odor threshold measured in adults, which purpose was to decrease odor annoyance. The U.S. EPA presently does not classify hydrogen sulfide as either a criteria air pollutant or a Hazardous Air Pollutant, however it has developed a chronic Reference Concentration (RfC) of 1 $\mu g/m^3$ for hydrogen sulfide (USEPA, 1999, 2003). The RfC is an estimate (with uncertainty spanning perhaps an order of magnitude) of a daily inhalation exposure of the human population (including sensitive subgroups) that is likely to be without an appreciable risk of deleterious noncancer effects during a lifetime (Collins and Lewis, 2000; USEPA, 2003).

2.6 H_2S Occupational Standards

The occupational exposure standards provide threshold limits for chemical substances in the working environment based on health effects safety guidelines. In Table 2-4, occupational exposure limits for H_2S from different international standards and safety limits are presented.

Table 2-4. International occupational safety guidelines for H_2S exposure.

Occupational standard	Limit value (ppm*)	Limit value ($\mu g/m^3$)	Exposure	Averaging period
ACGIH (2009)	10	14200	TLV-TWA	8 hour
	15	21300	TLV-STEL	15 minute
OSHA (2006)	20	28400	PEL-C	-
NIOSH (2005)	10	14200	REL-C	10 minute
European Commission (EC, 2009)	5	7100	TLV-TWA	8 hour
	10	14200	TLV-STEL	15 minute

* At 20°C and 1 atm, 1ppm = 1420 $\mu g/m^3$

The exposure is defined as follows,

Threshold Limit Value (TLV): exposure limit "to which it is believed nearly all workers can be exposed day after day for a working lifetime without ill effect" (ACGIH, 2009).

Time-Weighted Average (TWA): time-weighted average concentration for a conventional 8-hour workday and a 40-hour workweek, to which it is believed that nearly all workers may be repeatedly exposed, day after day, without adverse effect.

Short Term Exposure Limit (STEL): the concentration to which it is believed that workers can be exposed continuously for a short period of time without suffering from Irritation, chronic or irreversible tissue damage, or narcosis.

Permissible Exposure Limit (PEL-C): regulatory limit (ceiling) on the amount or concentration of a substance in the air, and they are enforceable.

Recommended Exposure Levels (REL-C): refers to the concentration that should not be exceeded during any part of the working exposure (ceiling).

3 Geological Setting

3.1 Regional Geology and Tectonic Setting

Nicaragua is located in the center of the Chortis block (Figure 3-1), one of the major structural units of the continental crust forming the Caribbean Plate (Weinberg, 1992). Volcanism in the region results from subduction of the Cocos Plate along the Central American Trench. A volcanic arc known as Central America Volcanic Arc (CAVA) extends along the Pacific coastline of the Central American Isthmus, from Guatemala in the northwest to Panama in the southeast (CNE, 2001).

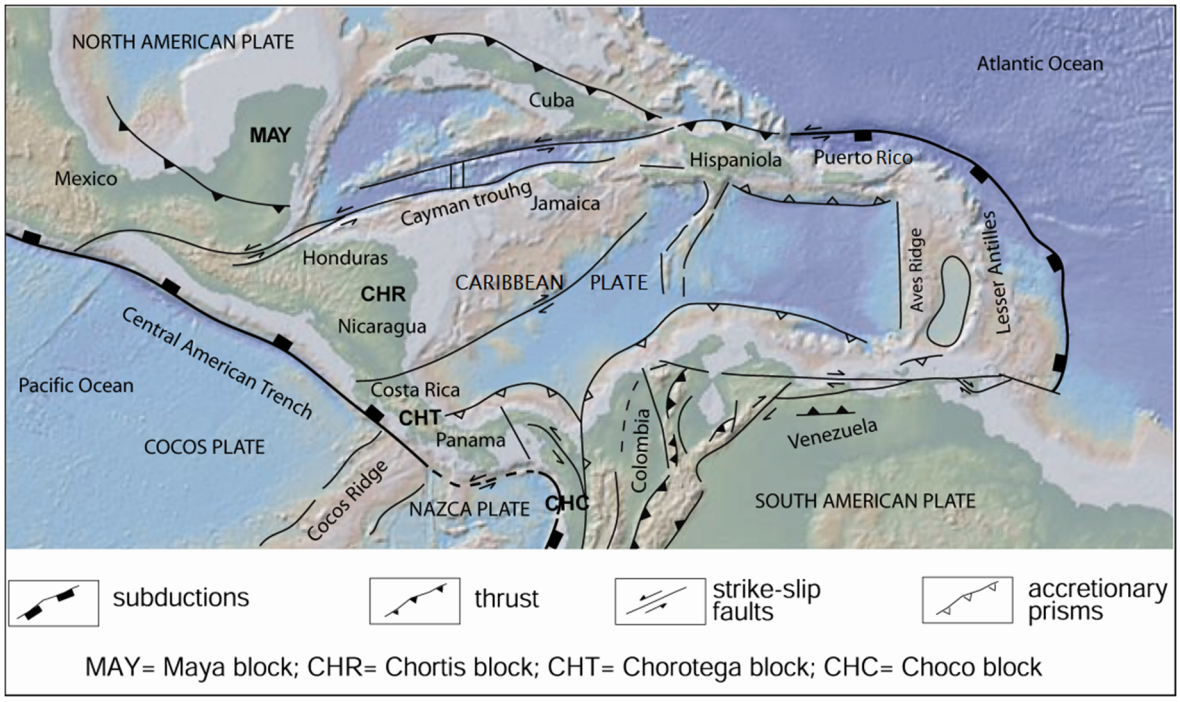

Figure 3-1. Tectonics of Central America and the Caribbean (modified from Giunta and Orioli, 2011).

The rate of subduction of the Cocos plate is amongst the fastest in the world at 8 cm/yr (Weinberg, 1992), with a comparatively steep angle of subduction of 60° (Gill, 1981). This angle is thought to have increased since the Pliocene, resulting in westward migration of the volcanic front (Weinberg, 1992).

The active volcanic arc with a NW-SE orientation in Nicaragua is known as Los Maribios range, occurring within the Nicaraguan depression. The Nicaraguan depression is a major tectonic structure parallel to the Central American Trench, which extends the length of western Nicaragua. The depression has been defined as a half-graben (a zone of structural subsidence) limited by NW-SW striking normal faults, generally dipping NE (McBirney and Williams, 1965).

Nicaragua is divided into four physiographical provinces, from west to east these are: The Pacific Coastal Plain, The Nicaraguan Depression, the Interior Highlands and the Atlantic Coastal Plain (McBirney and Williams, 1965). The stratigraphy of the Pacific Coastal Plain is divided into sequences of neritic sediments, mostly volcanoclastic deposited between the late Cretaceous and upper Miocene. Formations from this interval are folded, eroded and covered by carbonates and volcanic rocks of the Pliocene (Weinberg, 1992 and references therein). In the NW sector of the Pacific Plains, outcrops with thin layers of ignimbrites and lavas are found. The Nicaraguan Depression is partially covered by the Nicaragua and Managua Lakes (McBirney and Williams, 1965) and is filled by alluvial sediments and volcanic rocks (Weinberg, 1992).

3.2 The San Jacinto-Tizate Geothermal Field

The San Jacinto-Tizate geothermal field is located in northwestern Nicaragua, some 75 km NW from the capital Managua (Figure 3-2). The geological and tectonic history of the western region has been related to the geodynamic evolution of the pacific continental margin, characterized by subduction of the Cocos Ocean plate beneath the Caribbean Continental Plate (CNE, 2001).

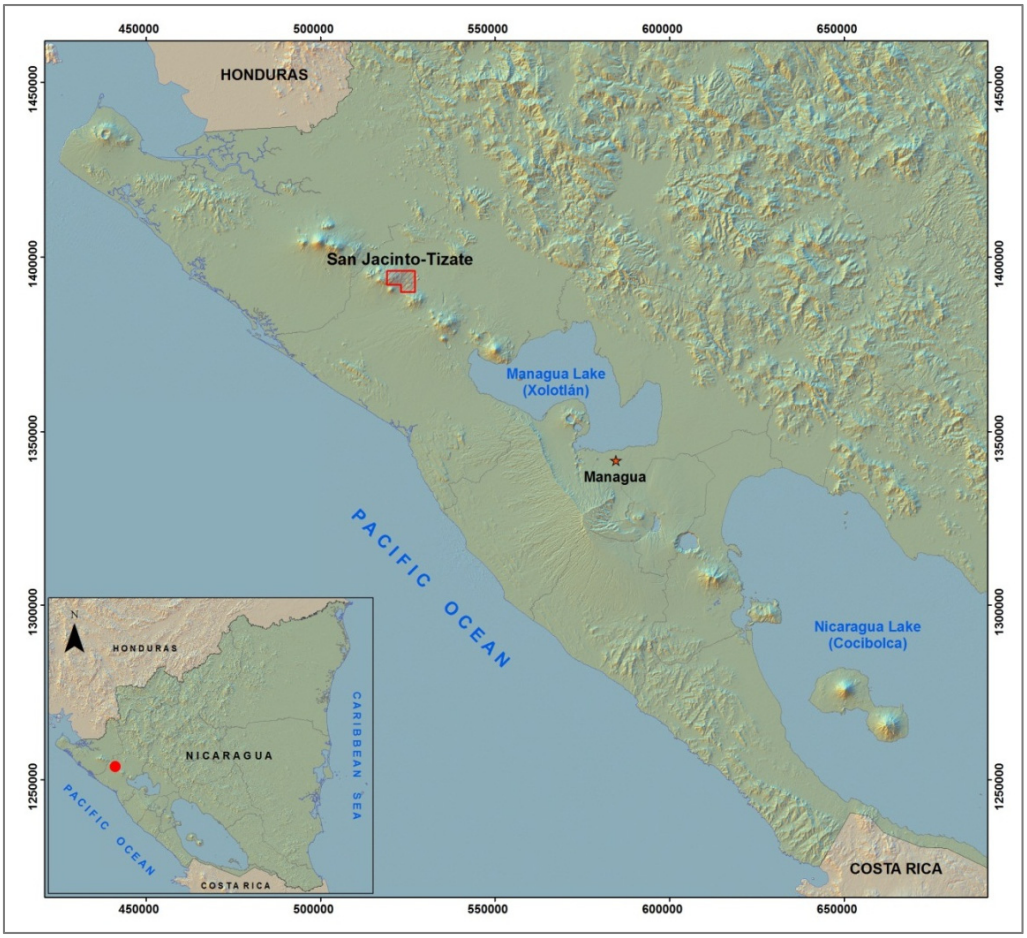

Figure 3-2. Location of San Jacinto-Tizate geothermal field (modified from MEM, 2008).

The closely spaced Quaternary volcanic centers in northwestern Nicaragua form a semi-continuous range, the Maribios cordillera. The San Jacinto-Tizate geothermal field lies on

the eastern part of the Telica volcanic complex which is located near the center of this range (Figure 3-2). The geothermal field comprises an active andesite volcano (Telica) at the northwest end with increasingly older volcanic centers to the southeast (White *et al.*, 2008). Thermal features comprise mud pools in the San Jacinto village and fumaroles and weak seasonal warm springs in the Tizate area to the north.

3.2.1 Geology and Stratigraphy

The San Jacinto-Tizate field constitutes the base of the eastern flank of the Telica volcanic massif (Figure 3-3). The eastern part of the Telica volcanic massif includes the lower slopes of San Jacinto volcano, Santa Clara volcano and the remains of the old volcanic edifice El Chorro. Other relatively old volcanic structures include the Rota volcano, located SSE of the geothermal field (CNE, 2001).

The surface geology of San Jacinto largely consist products from the surrounding volcanic centers of Telica, Santa Clara and Rota, which overlie a suite of older volcanic and epiclastic rocks that are locally intruded by porphyritic diorites. Similarly, extrusive volcanic rocks (lavas and tuffs) and related breccias, mainly of andesitic composition, with some intercalated volcanogenic sediments and intrusive diorites have been largely encountered in wells. There are not big differences in lithology between wells, but neither are there any beds that can be correlated across the field (White *et al.*, 2008).

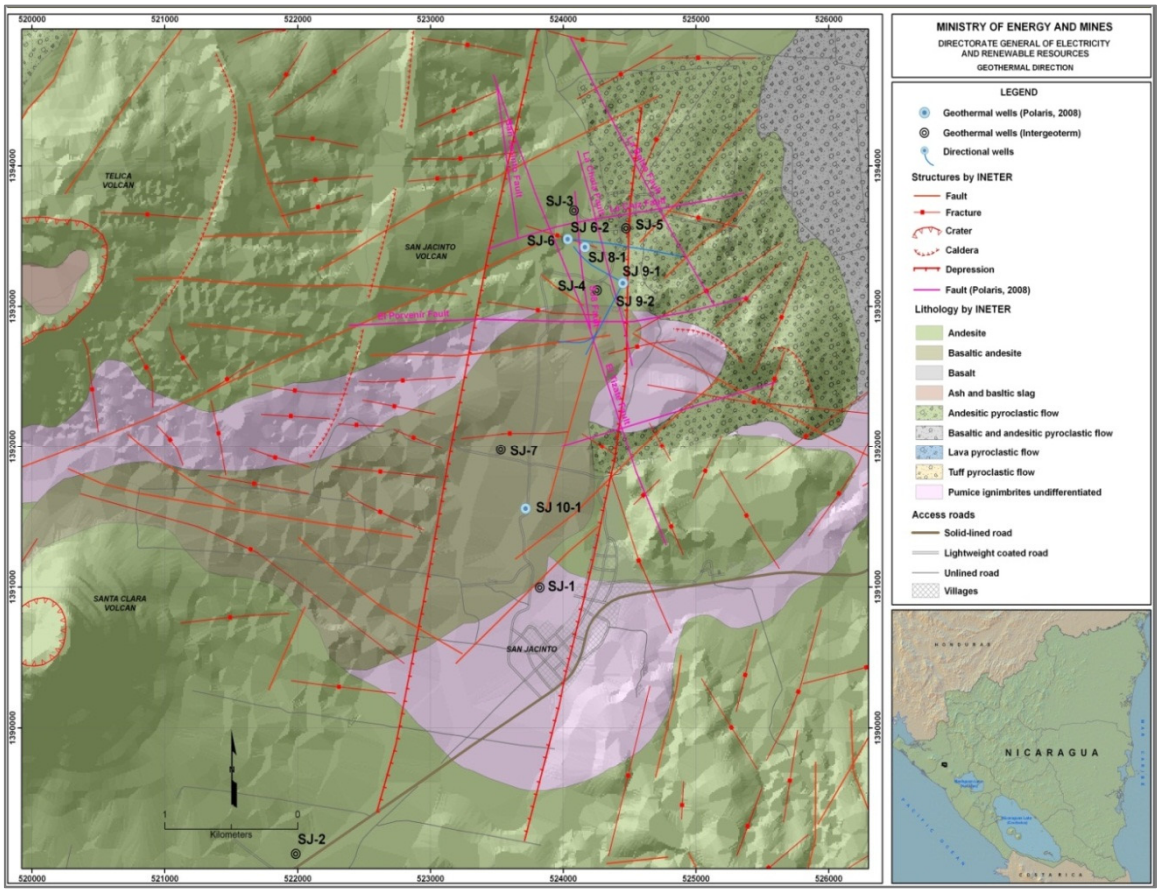

Figure 3-3. Geological map of San Jacinto-Tizate (MEM, 2008).

The geological succession of the field consists mostly of igneous, pyroclastic and intrusive rocks of basic-to-intermediate composition and sedimentary deposits of primary volcanic origin. The age of the rocks varies from late Miocene to Holocene. Different stratigraphic units have been identified, including pyroclastic-effusive units of the recent San Jacinto, Santa Clara and Rota volcanoes, a late Pleistocene unit of the El Chorro-Tizate volcano, the extrusive domes of Ignacio del Bosque, proluvial sediments of the San Jacinto Depression, and other units encountered only in the deep wells (Spektor, 1994).

According to Ostapenko *et al*. (1998), three main groups of faults have been identified in San Jacinto-Tizate: NNE-trending, NW-trending, and volcano-tectonic ring faults. The geothermal field is located within the composite structure formed by the superposition of the San Jacinto graben on the eastern part of the volcano-tectonic Telica Depression. The northern part of the structure (Tizate area) is intensively fractured by the intersection of faults with different trends.

3.2.2 Hydrothermal Alteration Mineralogy

Hydrothermal alteration is the mineralogical, textural and chemical response of the rocks when subjected to drastic changes in their formation environment. It is mainly dependent on permeability, temperature, pressure, rock types, fluid composition and duration of the activity (Browne, 1978). Hydrothermal alteration and mineralization are the results of an irreversible chemical exchange between an aqueous solution and adjacent rocks. Certain components are extracted selectively from the wall-rock and are added to the fluid and other components are selectively incorporated by secondary minerals and removed from the hydrothermal fluids.

The essential feature of the hydrothermal alteration is the conversion of a set of initial minerals into a new association of more stable minerals. Secondary minerals form by different hydrothermal alteration processes (replacement, leaching or deposition).

The formation of selected alteration minerals is mainly dependent on temperature. Table 3-1 presents the temperature stability ranges of selected alteration minerals present in geothermal fields in Nicaragua (SKM, 2008). Alteration mineralogy is widely used to analyze temperature conditions in a geothermal system and outline whether the system is in thermal equilibrium or whether heating or cooling has occurred.

Table 3-1. Formation temperature for alteration minerals.

Minerals	**Tmin (°C)**	**Tmax (°C)**
Zeolites	30	130-150
Laumontite	120	190-220
Wairakite	200	
Smectite	50	< 200
Mixed Layer Clay	200	230
Chlorite	230	≥300
Illite	230	≥300
Calcite	50-100	300
Quartz	160-180	≥300
Epidote	230-250	300
Actinolite	280	≥300

The hydrothermal alteration produces different alteration mineral assemblages in the rock at progressively increasing temperatures in the geothermal system. In the San Jacinto-Tizate geothermal field, hydrothermal alteration has been studied based on examination of drill cuttings. Depth-mineral zonation, which reflects the temperature stability of the hydrothermal minerals, is displayed at San Jacinto-Tizate in agreement with typically observed in high temperature geothermal systems.

According to White *et al.* (2008), five alteration assemblages have been identified in the wells drilled in San Jacinto-Tizate, although only three of these are common. With increasing depth from surface, these are:

1. Argillic: smectite and interlayered clays (chlorite-smectite and illite-smectite) are accompanied by zeolites (clinoptilolite, chabazite, epistilbite/heulandite, stilbite/mordenite), quartz, pyrite, iron oxides, calcite and chlorite, with rare opal and cristobalite. The zeolites are more or less zoned according to their temperature ranges in the shallower sections.

2. Mixed argillic-prophylitic: epidote is typically encountered at a depth of about 400-600 m, before illite replaces interlayered clays, meaning that instead of a purely phyllic zone, there is a zone of mixed argillic and prophylitic minerals.

3. Prophylitic: epidote is accompanied by minerals such as illite, laumontite, wairakite, adularia, prehnite, quartz, chlorite, calcite and pyrite.

4. High temperature prophylitic: rare amphibole, indicative of higher temperatures, occurs at depth in SJ9-2.

5. Contact metamorphic: minor biotite, amphibole and garnet were observed adjacent to diorite in SJ10-1.

Petrographic studies reveal disequilibrium mineral assemblages in all of the wells examined to date, with the coexistence of epidote with interlayered illite-smectite being one of the most obvious signs. This indicates that reservoir conditions have fluctuated over time (White *et al.*, 2008). The relatively low calcite content compared with the common presence of zeolites is consistent with low gas in the deep fluids, while the general absence of minerals such as alunite indicates that acid fluids are restricted in their distribution, if they occur at all in this part of the system (White *et al.*, 2008).

From the hydrothermal minerals reported in San Jacinto-Tizate geothermal system, of outmost interest to this study are the alteration minerals involved in controlling the activity of dissolved gases. In the case of H_2S these are: epidote, quartz, prehnite, pyrite, pyrrhotite, wollastonite, anhydrite and magnetite. A brief description is made bellow.

Epidote (Ca_2 (Al, Fe)$_3$ Si_3 (OH)) is a common mineral in geothermal reservoirs, being recognized as a key index mineral related to temperature, permeability, and fluid composition (Bird and Spieler, 2004). In well SJ9-2 at San Jacinto-Tizate, epidote is first identified at 600 m depth, increasing in abundance below 921 m depth. Epidote is usually associated with wairakite and quartz (Quintero-Roman, 2010).

The composition of epidote in active geothermal systems indicates a near complete solid solution between clinozoisite ($Ca_2Al_3Si_3(OH)$) and epidote ($Ca_2Al_2FeSi_3(OH)$), involving

substitution of Fe^{3+} for Al^{3+} on one of the three octahedral sites. The Fe end-member ($Ca_2Fe_3Si_3(OH)$) is referred to as pistachite and the composition of epidote minerals is commonly expressed in terms of mole fraction of pistachite (X_{ps}) which is defined as:

$$X_{ps} = \frac{n_{Fe}}{n_{Fe} + n_{Al}} \quad (1)$$

Epidote composition in San Jacinto-Tizate has not been reported to date.

Quartz (SiO_2) is commonly reported in all wells and through all depths. In well SJ9-2 quartz first appears around 129 m depth, as a small crystal (≥160-190°C). With increasing depth it occurs as euhedral and anhedral crystals, often replacing other minerals especially plagioclase or zeolite. It also occurs as vesicles fillings or as fine veins. In thin sections quartz is associated with epidote, calcite, wairakite and clay (Quintero-Roman, 2010).

Prehnite ($Ca_2Al_2Si_3O_{10}(OH)$) commonly occurs as a secondary mineral in basalts and related rocks. In well SJ9-2 at San Jacinto-Tizate appears as a small crystal at 681 m, where it is associated with epidote, being scarce in the entire well (Quintero-Roman, 2010).

Prehnite is a common mineral in geothermal fields, where it generally forms at temperatures between 250 and 350°C (Bird *et al.*, 1984). Prehnite composition depends on the substitution of ferric iron (Fe^{3+}) for aluminium (Al^{3+}) in the octahedral sites, defined as moles of Fe^{3+} per formula unit equivalent $X_{Fe,\ preh}=n_{Fe}$. The composition of prehnite in the San-Jacinto Tizate geothermal field has not been reported to date.

Pyrite (FeS_2) has been reported at different depths in well SJ9-2. The stratigraphy in the well consists primarily of interlayered andesitic lavas and tuffs, where pyrite is observed disseminated in the rock and also filling vesicles and veins (Quintero-Roman, 2010).

Anhydrite ($CaSO_4$) is a common mineral in saline geothermal areas or in sedimentary hosted geothermal system where inflow of fluid with a saline composition commonly results in the precipitation of anhydrite. This mineral was rare in SJ9-2, just observed in thin sections at 600 m and 1350 m depth (Quintero-Roman, 2010).

The hydrothermal minerals **wollastonite ($CaSiO_3$), pyrrhotite (FeS) and magnetite (Fe_3O_4)** have not been reported in the San Jacinto-Tizate wells.

3.2.3 Geochemistry

According to data from well testing and gas chemistry, the San Jacinto-Tizate is a liquid-dominated reservoir with outflows of steam and water to surface thermal areas (CNE, 2001). The deep fluid from the reservoir has been sampled from production wells, reporting a slightly alkaline, medium salinity, Na-Cl waters (CNE, 2001; White *et al.*, 2008). The chemistry for El Tizate wells is quite uniform, with calculated reservoir chloride concentrations falling in a range of 1,800 to 2,400 ppm and approximately neutral pH, typical of high temperatures hydrothermal systems developed in young volcanic rocks (CNE, 2001).

The composition of the gas dissolved in the deep liquid is represented by 95% in volume of CO_2 and 1% - 5% in volume of H_2S. The proportion of gases in the steam is of

approximately 0.5% to 1.5% in weight, and the concentration of H_2S in the steam is approximately 300 to 600 ppm in weight (CNE, 2001). The gas content in the steam from San Jacinto-Tizate reservoir has also been reported by IDB (2010), presenting a moderate low concentration (in production to date) with measured amounts of 0.45% in weight, from which only about 8% is H_2S. This represents an H_2S concentration of about 360 ppm in the steam.

4 Constraints on the H_2S Emission of the San Jacinto-Tizate Geothermal Power Plant

Detailed information on the concentration of dissolved gases in the steam from the San Jacinto-Tizate geothermal field was not available for this study, nor was the steam flow from wells and geochemistry of the deep liquid in the geothermal system. Therefore, an alternative method for estimating the content of dissolved gases in the geothermal fluid was used, being the gas of interest hydrogen sulfide (H_2S). The known installed capacity of the power plant (72 MW) and its estimated efficiency (in terms of MW per kg of steam) was used to estimate the steam flow. Mineral equilibrium considerations in the geothermal system are used to assess the H_2S concentration in the steam.

Fluids form geothermal systems contain dissolved gases, such as CO_2, H_2S, H_2, N_2, CH_4 and Ar. The concentration of individual gases vary depending on geological settings, temperature and composition of the geothermal reservoir (Gunnarsson *et al.*, 2013). The origin of the gases is either magmatic, meteoric or they are formed in the geothermal reservoir through water rock reactions. The dissolved gases can be either considered reactive and conservative constituents and have long been used by reservoir scientists to characterize the physical nature of the fluid and manage production from hydrothermal systems (e.g. Ármannsson *et al*., 1982; Gudmundsson and Arnórsson, 2002).

Production of fluids from high-temperature (>200°C) geothermal reservoirs by deep drillings has provided extensive information on the origin and chemistry of these fluids, the associated hydrothermal alteration and various hydrological characteristics of such systems (Karingithi *et al.*, 2010). Many studies carried out on the chemistry of the fluids discharged from wells have focused on evaluating the processes that control fluid compositions (e.g. Arnorsson and Stefansson, 1999; Arnórsson *et al.*, 1990; Arnórsson *et al.*, 1998; Arnórsson and Gunnlaugsson, 1985; Arnórsson *et al.*, 1983; D´Amore and Panichi, 1980; D´Amore and Truesdell, 1985; Giggenbach, 1980, 1981; Gudmundsson and Arnorsson, 2002, 2005; Nehring and Damore, 1984; Stefansson and Arnorsson, 2000) and some others on the source of specific chemical constituents in the fluid (e.g. Ármannsson *et al.*, 1982; Giggenbach, 1992).

Recent studies have successfully demonstrated that the gas concentration in geothermal well discharges is controlled by temperature-dependent equilibria between alteration minerals in the reservoir rock and gas concentration or gas ratios in the producing aquifer (Arnórsson and Gunnlaugsson, 1985).

Karingithi (2002) studied the state of equilibrium between the reactive gases and selected hydrothermal mineral buffers in the liquid-dominated, volcanic geothermal system Olkaria in Kenya. Subsequently, Karingithi *et al.* (2010) used chemical geothermometers to evaluate which processes controlled the aquifer fluid compositions in the same geothermal system. The approach largely focused on minerals that constitute assemblages that

potentially could control the aquifer liquid water concentration of the reactive gases, CO_2, H_2S and H_2.

González-Contreras (2010) also analyzed secondary mineral assemblages that could be involved in controlling the concentration of components present in the fluid such as CO_2, H_2S and H_2 in the Reykjanes Geothermal system, SW Iceland. In this study, the control of mineral buffers on the gas chemistry in the geothermal fluid was analyzed, determining trends of gas concentration as a function of temperature.

A similar approach can be used to estimate H_2S gas concentration in the deep liquid from the San-Jacinto Tizate geothermal system, given the alteration mineralogy and temperature reported for this geothermal field. In the following sections, the method applied to constrain the H_2S concentration in the deep liquid and steam in the geothermal system under study is depicted.

4.1 Thermodynamics and Mineral Equilibria

Many authors have postulated about the equilibrium of mineral assemblages in controlling the activity of dissolved gases at geothermal systems. Stefánsson and Arnórsson (2002) propose mineral buffers likely to control the activity of CO_2, H_2S and H_2 for saline geothermal fluids. Arnórsson *et al.* (1998), Stefánsson and Arnórsson (2002) and Freedman *et al.* (2009) agree in that the mineral buffer of epidote, calcite, quartz and prehnite controls the activity of CO_2. For H_2S and H_2 gases, Arnórsson *et al.* (1998) propose a mineral assemblage involving pyrite, pyrrhotite, epidote and prehnite, and Stefánsson and Arnórsson (2002) suggest mineral assemblages for saline geothermal fluids including pyrite, prehnite, magnetite, anhydrite, clinozoisite and quartz for H_2S and H_2.

Here the activity of dissolved H_2S in the deep geothermal liquid from the San Jacinto-Tizate geothermal system is predicted assuming equilibrium with the mineral assemblages proposed by González-Contreras (2010) and Karingithi *et al*. (2010), as follows: pyrite, pyrrhotite, prehnite and epidote; pyrite, pyrrhotite and magnetite; wollastonite, pyrite, anhydrite, quartz and magnetite; prehnite, pyrite, clinozoisite, anhydrite, quartz and magnetite.

The following balanced chemical reactions represent mineral buffers that may control H_2S in a given geothermal system:

(a) $\frac{1}{3}FeS_2 + \frac{1}{3}FeS + \frac{2}{3}Ca_2Al_2Si_3O_{10}(OH)_2 + \frac{2}{3}H_2O = \frac{2}{3}Ca_2Al_2FeSi_3O_{12}(OH) + H_2S_{aq}$

(b) $\frac{1}{4}FeS_2 + \frac{1}{2}FeS + H_2O = \frac{1}{4}Fe_3O_4 + H_2S_{aq}$

(c) $CaSiO_3 + 6FeS_2 + 11H_2O = CaSO_4 + SiO_2 + 2Fe_3O_4 + 11H_2S_{aq}$

(d) $3Ca_2Al_2Si_3O_{10}(OH)_2 + 12FeS_2 + 20H_2O = 2Ca_2Al_3Si_3O_{12}(OH) + 2CaSO_4$

$$+3SiO_2 + 4Fe_3O_4 + 22H_2S_{aq}$$

Each of these reactions was solved numerically for gas concentration for a given temperature. Equilibrium constants (K) as a function of temperature were computed using

SUPCRT92 software (Johnson *et al.*, 1992) for reactions **c** and **d**. In the case of reactions **a** and **b**, *K* was computed based on temperature equations for equilibrium constants presented by Karingithi *et al.* (2010) for the selected mineral assemblage reactions. The computed equilibrium constants are presented in Appendix A.

For the evaluation of mineral control of gas concentration, the activity of dissolved species is calculated. The aqueous solutions composition presented in terms of molality, (m) is related to the activity (a_i) by an activity coefficient (γ_i).

$$a_i = m_i * \gamma_i \quad (2)$$

The activity model most commonly used in geochemical studies (Debye-Huckle model) assumes that the natural logarithm of the activity coefficient of a given dissolved species is a function of its charge. As a result the value of the activity coefficient for the uncharged species is equal to unity and thus the activity equal to molality.

Hydrothermal minerals such as quartz (SiO_2), calcite ($CaCO_3$), pyrite (FeS_2), pyrrhotite (FeS), anhydrite ($CaSO_4$), magnetite (Fe_3O_4), wollastonite ($CaSiO_3$) and water were considered to be pure and therefore their activity equal to 1. In the case of solid solutions as prehnite ($Ca_2Al_2Si_3O_{10}(OH)_2$) and epidote ($Ca_2(Al,Fe)_3Si_3O_{12}(OH)$), activity values were computed from data published by Bird and Spieler (2004), where the mineralogical characteristics and composition of epidote in active geothermal systems by global tectonic setting is presented.

In the case of convergent plate boundaries of the Circum-Pacific Margin, where Central America is located, epidote and prehnite composition from Miravalles geothermal system in Costa Rica has been reported. For this study, the composition from the above mentioned minerals in Miravalles geothermal system was deemed to be representative of the San Jacinto- Tizate geothermal system in Nicaragua, given the similarity of geothermal areas located within the same region.

In the Miravalles geothermal field, epidote compositions range from X_{ps}=0.18 - 0.32, and prehnite from X_{Fe}=0.04 - 0.24 (Bird and Spieler, 2004). A mean value for composition of epidote X_{ps}=0.25 and prehnite X_{Fe}=0.14 was used for obtaining the following activity values: $a_{ep}\approx0.75$, $a_{Czo}\approx0.25$ and $a_{Preh}\approx0.86$.

For the mineral buffers considered to be controlling H_2S, equilibrium constants were used according to the following principle in terms of activities of the species, which values were explained above.

$$\alpha A + \beta B = \gamma C + \delta D \quad (3)$$

$$K = \frac{[C]^{\gamma}[D]^{\delta}}{[A]^{\alpha}[B]^{\beta}} \quad (4)$$

The predicted concentrations of H_2S as a function of temperature in the deep liquid for each mineral buffer considered is calculated for the reported temperatures in San Jacinto-Tizate geothermal system, 250-290°C (Figure 4-1). Reactions for reduced conditions in the geothermal system (lines **a** and **b** in Figure 4-1) predict high H_2S concentration values, while reactions for oxidized conditions (lines **c** and **d)** predict low concentration values.

The variation in the predicted concentration depends on the mineral assemblages controlling H_2S in the geothermal system. Different scenarios can be inferred depending of the conditions in the geothermal system. The low concentrations predicted by reactions **c** and **d**, are representative of geothermal systems controlled by oxidized conditions, as is the case of saline geothermal systems.

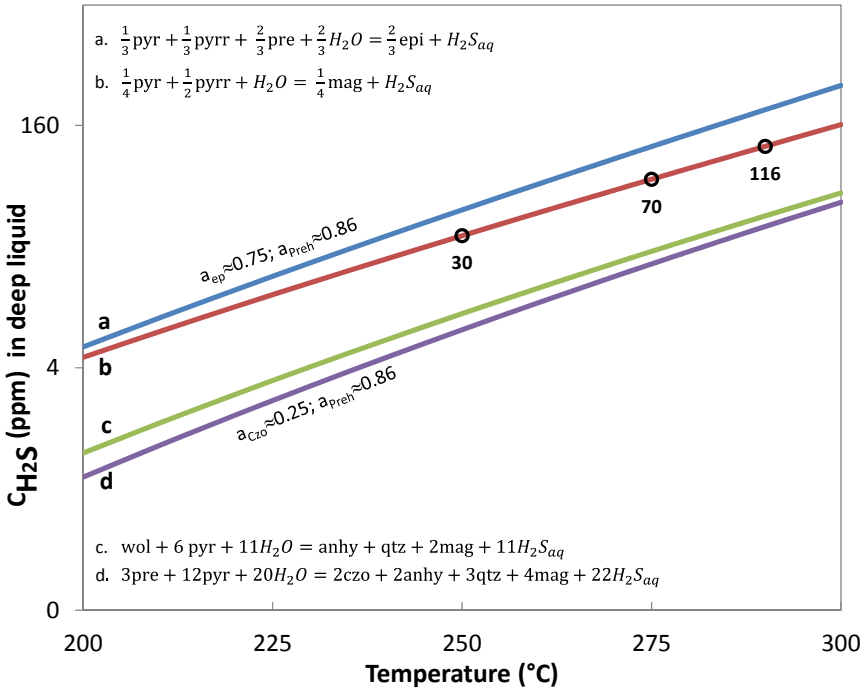

Figure 4-1. H_2S gas concentration in the deep liquid as a function of temperature for theoretical mineral equilibrium, where lines a and b represent reduced conditions and lines b and c, oxidized conditions.

The concentration of H_2S in the San Jacinto-Tizate geothermal system is assumed to be controlled by mineral assemblages considered in reaction **b** (reduced conditions), which represents the second worst case scenario for H_2S emissions. Highly reduced conditions, represented by reaction **a**, have not been reported for the San Jacinto-Tizate geothermal field.

4.2 Concentration of H_2S in Steam

Given the concentration of H_2S in the deep liquid from San Jacinto-Tizate geothermal system, the H_2S concentration in the steam can be computed under the assumption that all the gas is contained in the steam phase when the deep liquid boils. The gas concentration corresponds to the ratio between the concentration in the deep fluid and the steam fraction correspondent to a reference temperature and pressure.

The steam fraction was computed based on the following assumptions:

- The temperature of the deep liquid in San Jacinto-Tizate ranges from 250-290°C.
- The geothermal system is liquid dominated.

- The separation pressure set to 10 bar-a.
- Boiling in the geothermal system is taken to be adiabatic, when the fluid rises to the surface it boils due to reduced hydrostatic pressure.
- Conservation of enthalpy, assuming that no heat or mass is lost or gained to the environment when the fluid rises. The enthalpy content in the fluid is constant.

The steam fraction is computed in terms of enthalpy by the following equation,

$$X = \frac{h_t^{dl} - h_{ps}^{l}}{h_{ps}^{s} - h_{ps}^{l}} \quad (5)$$

where *h* refers to enthalpy, the superscripts *dl, l* and *s* refer to deep liquid, liquid and vapor phases, respectively. Subscripts refer to reference temperature (*t*) and separation pressure (*ps*). For the considered temperature range the calculated steam fraction varies from 0.160 to 0.262 (Table 4-1).

Table 4-1. Reference temperatures and calculated steam fraction.

Temperature (°C)	Steam *X* at 10 bar-a
200	0.045
210	0.067
220	0.090
230	0.113
240	0.136
250	0.160
260	0.185
270	0.210
275	0.222
280	0.235
290	0.262
300	0.289

The H_2S gas concentration in steam was calculated from the following equation, assuming all the gas is contained in then steam phase,

$$m_i^{dl} = X m_i^{s} + \cancelto{0}{(1 - X) m_i^{l}} \quad (6)$$

$$m_i^{s} = \frac{m_i^{dl}}{X} \quad (7)$$

Where m_i refers to the concentration of the gas *i*, the superscripts, *dl*, *s*, and *l* refer to deep liquid, steam phase and liquid phase, respectively and *X* refers to the steam fraction for the reference conditions.

For the purpose of the present study, the concentration of H_2S in San Jacinto-Tizate geothermal system is assumed to be controlled by reaction **b** (Figure 4-2). Taking reaction **b** as reference, the predicted concentration of H_2S in steam will be 64% higher if the

system is controlled by minerals in reaction **a**; and 67% and 73% lower if H_2S is controlled by minerals in reaction **c** and **d** respectively.

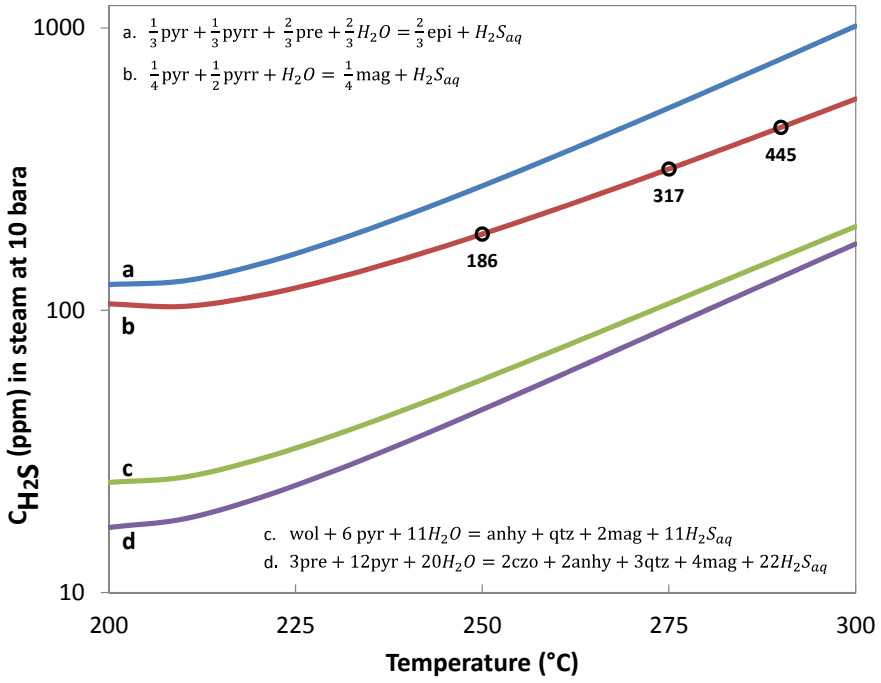

Figure 4-2. H_2S concentration in the steam from San Jacinto-Tizate geothermal system, where lines a and b represent reduced conditions and lines b and c, oxidized conditions.

In the San Jacinto-Tizate geothermal field, a temperature in the range of 250-290°C has been reported in boreholes. Assuming that the mineral assemblages considered in reaction **b** represent the conditions in the geothermal system, a concentration of H_2S in steam in the range of 186-445 ppm is predicted. In this study, a mean temperature of the deep liquid at 275°C is assumed, resulting in a concentration of 317 ppm of H_2S in the steam. This value is within the H_2S concentration range of 300-600 ppm reported by CNE (2001) in the steam from San Jacinto-Tizate geothermal field, and in agreement with the concentration reported by BID (2010) of 360 ppm of H_2S in the steam.

4.3 H_2S Emissions from San Jacinto-Tizate Power Plant

The known installed capacity of the power plant (72 MW) and its estimated efficiency (in terms of MW per kg of steam) is used to estimate the steam flow. Given the concentration of H_2S at 317 ppm in the steam and a steam consumption of 2 kg/s per MW in a standard condensing turbine (Figure 4-3), the H_2S emissions from San Jacinto-Tizate power plant when it operates at full load for a whole year is estimated as 1436.2 tons/year, or an emission rate of 45.5 g/s.

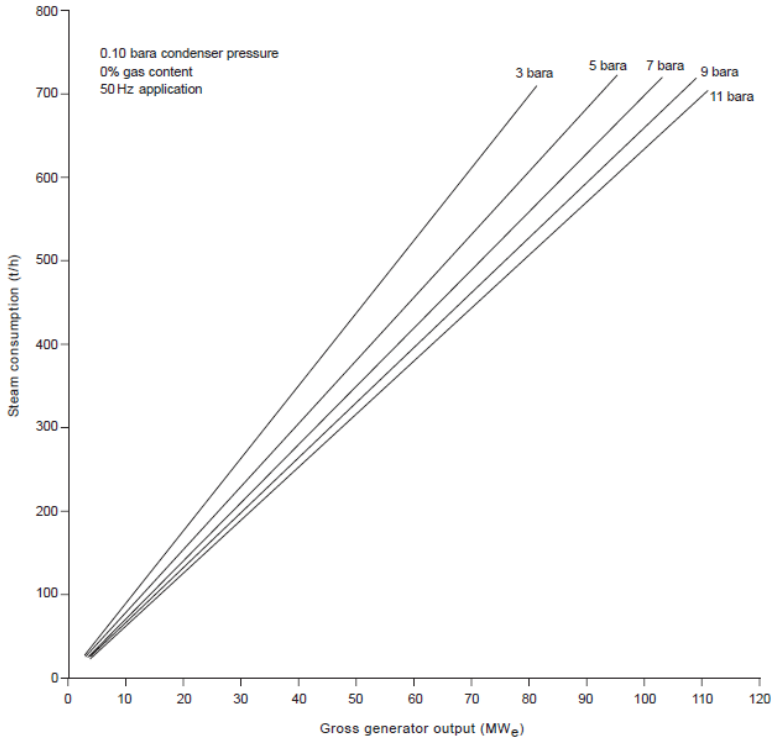

Figure 4-3. Condensing turbine steam consumption curves (Dickson and Fanelli, 2003).

In the San Jacinto-Tizate geothermal power plant, 2x36 MW condensing turbines were commissioned in 2012. The steam exhaust from the turbines passes through a condenser which produces a condensate stream and a non-condensable gas stream. The non-condensable gases (including H_2S) are vented out of the condensers to atmosphere in the cooling towers to enhance dispersion (Figure 4-4).

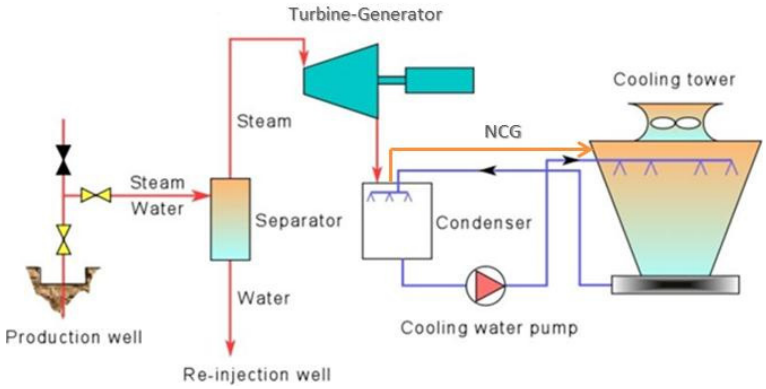

Figure 4-4. Simplified schematic of the condensing cycle at the San Jacinto-Tizate geothermal power plant (modified from Dickson and Fanelli, 2004).

5 Dispersion Modeling

This chapter comprises the different steps needed to carry out the dispersion modeling study. First the emission data from San Jacinto-Tizate power plant is presented, then the meteorological data used in the model and the reported H_2S concentration measurements in the vicinity of the power plant are described. Finally the simple Gaussian plume approach used in this study and AERMOD dispersion model is described.

5.1 Input Data

5.1.1 Source Emissions Data

The concentration of hydrogen sulfide in the steam of San Jacinto-Tizate was computed as described in Chapter 4. The emission rate when the power plant operates at full load (72MW) was estimated as 45.5 g/s.

The stack characteristics were defined according to the configuration of the San Jacinto-Tizate Power Plant. The H_2S emissions are made through the cooling towers. The NCG are discharged below the cooling tower fans to ensure mixing with the air and steam as it is blown high into the atmosphere. The H_2S is then mixed in the plume emitted through five closely spaced outlets in the cooling tower. There is a cooling tower for each 36 MW condensing unit in San Jacinto-Tizate Power Plant. The cooling tower outlets are modeled as one point source with a combined area. The stack inside diameter was estimated as 24.6 m for each cooling tower.

Based on preliminary design parameters of the San Jacinto-Tizate power plant reported by Ingimundarson and Thorhallsson (2012), the gas temperature used is the steam temperature in the cooling tower exhaust (~40°C) and the gas exit velocity was estimated from the airflow through the cooling towers based on a simplified scheme of the cooling needs in the system (condenser-cooling towers). The gas exit velocity is approximately 3 m/s.

5.1.2 Meteorological Data

Meteorological data is needed to calculate air pollution distribution. For this study, hourly measurements of wind speed, wind direction, air temperature, pressure, relative humidity and precipitation from the weather station run by the project developer, PENSA in the San Jacinto-Tizate power plant site were obtained for the period January 2012 to June 2013. Cloud cover is not measured in the station at the project site; therefore cloud cover reports for the same period were obtained from León weather station (code 64043), run by Nicaraguan Institute for Territorial Studies (INETER) 22 km west of the project site.

The Leon weather station is a manned observation station and cloud cover measurements are just reported for day time (10 hours a day). Night time cloud cover for the modeling period was estimated using a linear interpolation function available within R statistic software (R Core Team, 2013).

Weather data processing from the SJT weather station included the use of linear interpolation methods to fill gaps in different meteorological parameters. The methodology recommended by the EPA regarding "Procedures for substituting values for missing NWS Meteorological Data for use in regulatory air quality models" was used whenever possible. According to this method, a data set which is less than 90% complete should not be used for air quality modeling purposes (Atkinson and Lee, 1992).

Predominant wind speed and direction was identified in the project area (Figure 5-1). The mean wind speed reported is 3 ± 2 m/s, with prevailing ENE (15.6% of the time), E (14%) and SSW (13.7%) winds. The average air temperature is 27 ± 3°C and the average relative humidity (RH) 63 ± 16%.

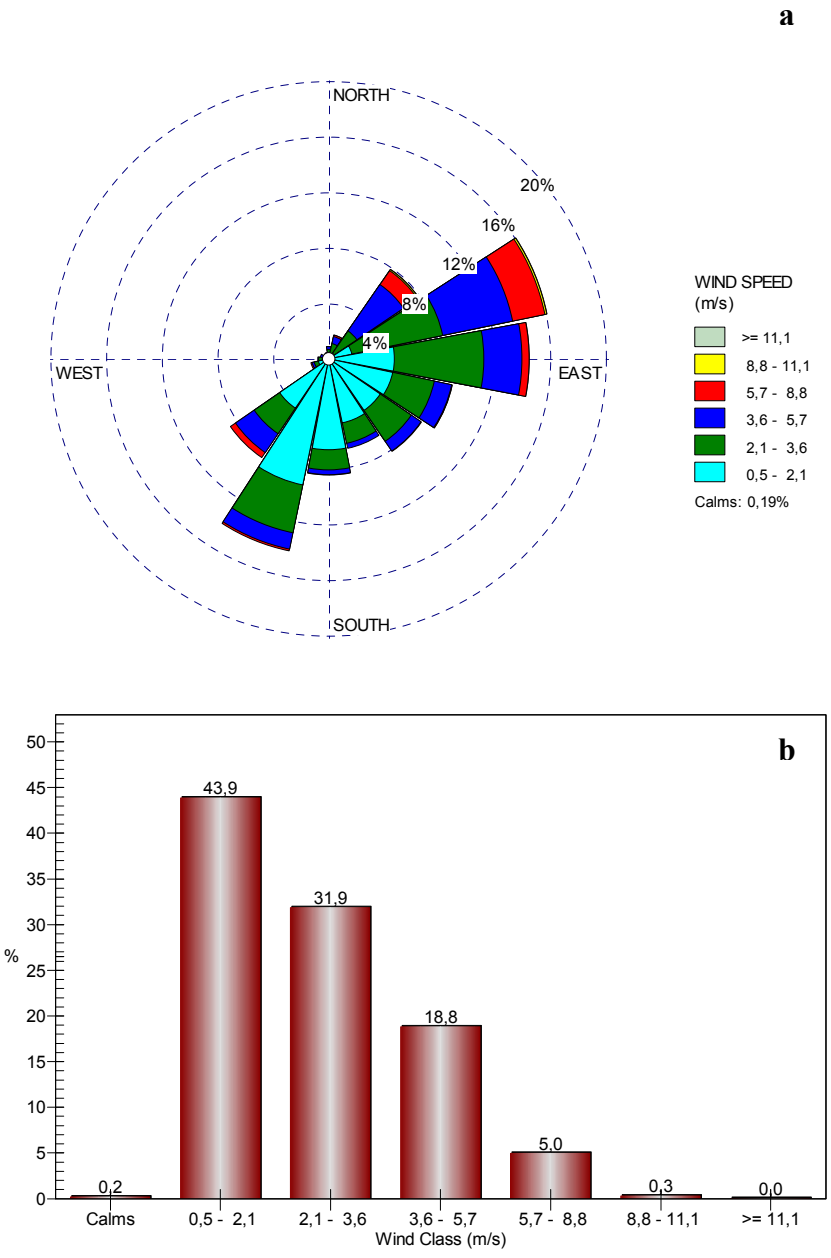

Figure 5-1. a) Wind rose for the SJT weather station January-December 2012, b) Wind class frequency distribution.

5.1.3 Concentration of H_2S in the Project Area

The San Jacinto-Tizate Project developer (PENSA) implemented an Air Quality Monitoring program since 2006. Hydrogen sulfide ambient air concentration levels are measured and reported twice a year around well platforms, power plant and some receptors.

For each monitoring cycle, measurements of H_2S concentration at approximately 1-hour interval are made during periods of 24 hours. A Jerome 631-X Hydrogen Sulfide Analyzer, with a detection range of 0.003-50 ppm or 4.26-71000 $\mu g/m^3$ (Arizona Instrument LLC, 2014) is used for the measurements. Only the averaged concentrations from each monitoring period are reported to regulatory bodies.

In this study, the average concentration at different monitoring points (Table 5-1) is used for comparison purposes with predicted concentrations from dispersion modeling. The power plant installed capacity and operation conditions during each monitoring period were different. In March 2012, the installed capacity of the plant was 46 MW (2x5 MW backpressure units and 1x36 MW condensing unit) with a highly variable electricity generation (10-40 MW). In September 2012 and June 2013 the installed capacity was 72 MW (2x36 MW condensing units) with a steady electricity generation, 38 MW and 59 MW respectively.

Table 5-1. Reported H_2S concentrations in the project area (PENSA, 2012, 2013).

Monitoring points/receptors	Average concentration ($\mu g/m^3$)		
	6 - 7 March 2012	19 - 20 September 2012	6 - 7 June 2013
SJ-11	1.42	1.99	0.99
SJ-12	2.84	4.12	3.27
SJ-4	5.68	6.11	2.98
SJ-5	15.62	8.66	3.12
SJ-6	22.72	6.39	2.27
SJ-9	5.68	5.68	2.41
El Tizate	2.13	2.70	1.70
Receptor A	2.56	2.56	0.99
Pumping Station	22.58	11.22	2.84
Cooling Tower	19.88	3.27	5.25
Power Plant U1,2	28.83	-	-
Power Plant U3	30.10	2.98	3.69
Power Plant U4	-	-	3.55

5.2 Gaussian Plume Dispersion Model

The Gaussian plume model is the most common air pollution model for single and multiple sources. It is based on a material balance where a point source is considered and a downwind concentration is computed. In this project a simple Gaussian plume approach is used by assuming the plume travels straight downwind from the source and no obstacles or

terrain interfere in its way. The calculation is made to analyze the effect of distance and atmospheric stability on ground level concentration in the San Jacinto-Tizate project area.

The three dimensional concentration field generated by a point source, under stationary meteorological and emission conditions, is called a plume (Figure 5-2). The origin of the coordinate system is placed at the base of the smokestack with the x axis aligned in the downwind direction. The plume is assumed to be emitted from a point with coordinates (0, 0, *H*) where *H* is the effective stack height which is the sum of the physical height and the height to which the plume rises before levelling off. For a thin sheet of air that extends a certain distance in the *x* direction, to infinity in the *y* and *z* directions and moves with the local wind speed, materials are transferred up and downwind of it by turbulent dispersion. Assuming negligible net transfer in the *x*-direction makes the spreading problem two-dimensional (Nevers, 2000).

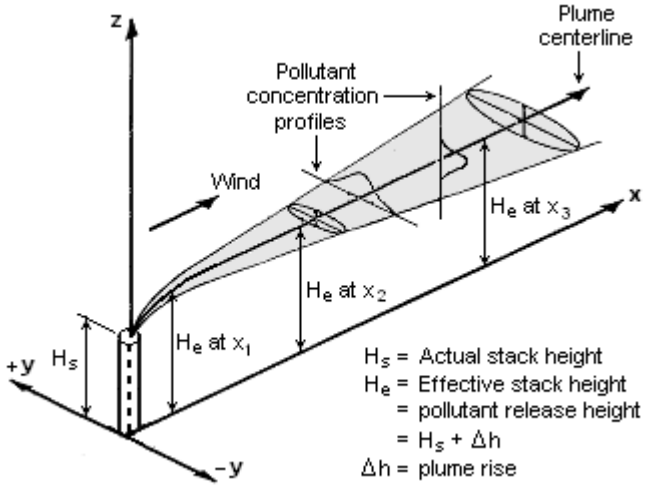

Figure 5-2. Gaussian plume schematic representation (BMacZero, 2012).

5.2.1 Gaussian Plume Equation

The basic Gaussian equation estimates the concentration at a receptor located at *x* downwind, *y* crosswind, and at a height *z* above the ground that results from a point source with an effective stack height *H* above the ground (Nevers, 2000). The basic Gaussian equation is:

$$X = \frac{Q}{2\pi\sigma_y \sigma_z u_h} \exp\left[-\frac{y^2}{2\sigma_y^2}\right] \exp\left[\frac{(z-H)^2}{2\sigma_z^2}\right] \quad (8)$$

where *X* is the air pollutant concentration in mass per volume (g/m^3), *Q* is the pollutant emission rate in mass per time unit (g/s), u_h is the wind speed at stack height (m/s), σ_y is the standard deviation of the concentration distribution in crosswind direction at the downwind direction x (m), σ_z is the standard deviation of the concentration distribution in vertical direction at the downwind direction *x* (m), *y* is the horizontal distance from the receptor to the plume center, *z* is the vertical distance from the receptor to the plume center and *H* is the effective height of the centerline of the pollutant plume (m).

The wind speed at stack height is calculated from the equation by Schulman and Scire (1980):

$$u_h = u\left(\frac{z_h}{z}\right)^P \quad (9)$$

where u_h is the wind speed at stack height, u is the measured wind speed, z_h is the physical stack height, z is the height at which the wind speed is measured and P is the wind shear exponent. P is dependent on the air stability class (see Section 5.2.2) and its value can be found in Table 5-2.

Table 5-2. Values for the wind shear exponent, P (Schulman & Scire, 1980).

Stability Class	P
A	0.10
B	0.15
C	0.20
D	0.25
E	0.30
F	0.30

The Gaussian distribution equation requires only two dispersion parameters (i.e. σ_y and σ_z) to identify the variation of pollutant concentrations away from the center of the plume. This distribution equation determines ground level pollutant concentrations based on time-averaged atmospheric variables (e.g. temperature, wind speed) under the assumption that the pollutant concentration in the plume is normally distributed as shown in Figure 5-3 (USEPA, 2005).

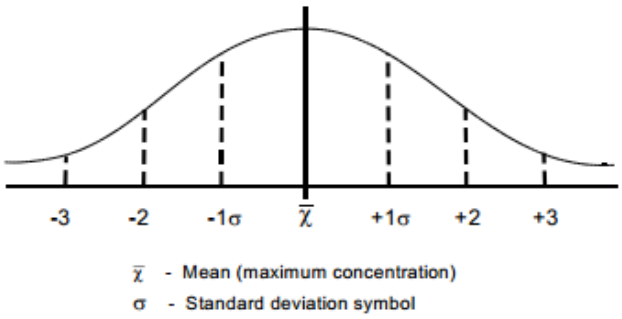

Figure 5-3. Gaussian distribution (USEPA, 2005).

While the plume travels it spreads and reaches the surface of the ground, being reflected. The Gaussian equation for the concentration with a mirror-image plume is,

$$X = \frac{\mathrm{Q}}{2\pi\sigma_y\sigma_z u}\exp\left[-\frac{y^2}{2\sigma_y^2}\right]\left(\exp\left[-\frac{(z-H)^2}{2\sigma_z^2}\right] + \exp\left[-\frac{(z+H)^2}{2\sigma_z^2}\right]\right) \quad (10)$$

For a ground level receptor, the equation becomes,

$$X = \frac{\mathrm{Q}}{\pi\sigma_y\sigma_z u}\exp\left(-\frac{y^2}{2\sigma_y^2}\right)\exp\left(-\frac{H^2}{2\sigma_z^2}\right) \quad (11)$$

5.2.2 Stability Classification

The stability of the atmosphere depends on temperature difference between an air parcel and the air surrounding it. Therefore, different levels of stability can occur based on how large or small the temperature difference is between the air parcel and the surrounding air (USEPA, 2005). For dispersion estimation and modeling purposes, the atmosphere stability is classified into six classes: A= Extremely unstable, B= Moderately unstable, C= Slightly unstable, D= Neutral, E= Slightly stable, F= Stable.

The stability classes are referred to as **Pasquill-Gifford stability classes (**Table 5-3**)** and are based on five surface wind speed categories, three types of daytime insolation, and two types of night-time cloudiness.

Table 5-3. Atmospheric stability classification.

Surface wind[a] m/s	**Day solar insolation**			**Night cloudiness**	
	Strong[b]	**Moderate[c]**	**Slight[d]**	**Cloudy >4/8**	**Clear <3/8**
<2	A	A-B	B	E	F
2-3	A-B	B	C	E	F
3-5	B	B-C	C	D	E
5-6	C	C-D	D	D	E
>6	C	D	D	D	D

[a] at 10 m above ground, [b] sun higher than 60º and clear sky, [c] sun 35-60º and few broken clouds or clear sky, [d] sun 15º-35º and cloudy.

5.2.3 Plume Dispersion Coefficients

The basic Gaussian equation predicts a plume that is symmetrical with respect to *y* and *z*. The standard deviation parameters of the concentration distribution in horizontal and crosswind direction (σ_y and σ_z respectively) are called horizontal and vertical dispersion parameters and are dependent on the air stability and the distance from the source. When the dispersion coefficients increase the centerline concentration decreases and the plume can be detected farther away from the plume center (Nevers, 2000; Turner, 1994).

These σ_y and σ_z dispersion coefficients have units of meters and correspond to an air pollutant sampling time of 10 minutes. The dispersion coefficients are function of the atmospheric stability class and the downwind distance *x* from the air pollutant emission source. The magnitude of the σ_y and σ_z dispersion coefficients in meters can be estimated using the equations reported by Martin (1976),

$$\sigma_z = cx^d + f \quad , \quad \sigma_y = ax^b \quad (12)$$

Values for four of the stability dependent constants (*a, c, d*, and *f*) are given in the Table 5-4. There are different values for the constants as a function of the downwind distance *x*. The value for *b* is constant = 0.894.

Table 5-4. Values of a, c, d, and f for calculating σ_y and σ_z (Martin, 1976).

Stability Class		$x \leq 1$ km			$x \geq 1$ km		
	a	***c***	***d***	***f***	***c***	***d***	***f***
A	213	440.8	1.041	9.27	459.7	2.094	-9.6
B	156	106.6	1.149	3.3	108.2	1.098	2.0
C	104	61.0	0.911	0.0	61.0	0.911	0.0
D	68	33.2	0.725	-1.7	44.5	0.516	-13.0
E	50.5	22.8	0.675	-1.3	55.4	0.305	-34.0
F	34	14.35	0.740	-0.35	62.6	0.180	-48.6

5.2.4 Plume Rise

The gases emitted thorough stacks and cooling towers are pushed out by fans. As the turbulent exhaust gas exit the stack it mixes with ambient air. This mixing of ambient air into the plume is called entrainment, causing the plume diameter to grow as it travels downwind. The gas has momentum as it enters the atmosphere. When the gas is warmer than the outdoor air, it is less dense than the outside air and is therefore buoyant (USEPA, 2005).

A combination of the gas momentum and buoyancy causes the gas to rise. This is referred to as plume rise and allows air pollutants emitted in the gas stream to be lofted higher in the atmosphere. Since the plume is higher in the atmosphere, it will disperse more before it reaches ground level (USEPA, 2005). The final height of the plume, referred to as the effective stack height H, is the sum of the physical stack height and the plume rise Δh. The plume rise is the height to which the plume rises before levelling off.

The plume rise is found for the buoyant and momentum rise and the plume rise is taken as the higher rise of the two. The buoyancy flux is used to calculate buoyant rise, which can be obtained from the equation reported by Turner (1994),

$$F = gvd^2\Delta T/(4Ts) \quad (13)$$

where F is the buoyancy flux (m^4/s^3), g is the acceleration of gravity (9.8 m/s), v is the stack gas exit velocity (m/s), d is the top inside stack diameter (m), ΔT is the stack gas temperature minus ambient air temperature (K) and Ts is the stack gas temperature (K).

In San Jacinto-Tizate geothermal power plant, the gas is emitted from the cooling towers as described in Section 5.1.1. The diameter and exit velocity of the steam from the cooling towers is used to calculate the buoyancy flux.

For unstable or neutral conditions the buoyant rise can be calculated from the following two equations:

For buoyancy flux less than 55 (F<55),

$$\Delta h = 21.425 \frac{F^{3/4}}{u_h} \quad (14)$$

and for F>55,

$$\Delta h = 38.71 \frac{F^{3/5}}{u_h} \quad (15)$$

where Δh is the plume rise and u_h is the wind speed at stack top

The momentum rise is calculated by,

$$\Delta h = \frac{3dv}{u_h} \quad (16)$$

where the parameters are defined as before. The buoyant rise and momentum rise values are compared and the larger one is used for unstable and neutral conditions.

For buoyant rise in stable air a stability parameter, s, is evaluated (Turner, 1994),

$$s = g \frac{d\theta/dz}{T_a} \quad (17)$$

where g is the acceleration of gravity (9.8 m/s^2), $d\theta/dz$ is the change of potential temperature with height (K/m) and T_a is the ambient air temperature (K).

If the change of potential temperature with height is not known, the following values can be used:

$d\theta/dz$ =0.02 °K m^{-1} for E stability

$d\theta/dz$ =0.035 °K m^{-1} for F stability

The stable buoyant rise is then calculated from the following two equations,

$$\Delta h = 2.6 \left(\frac{F}{u_h s} \right)^{1/3} \quad (18)$$

and

$$\Delta h = 4 \frac{F^{1/4}}{s^{3/8}} \quad (19)$$

The lower of these two is then used to compare to the stable momentum rise. The stable momentum rise is also calculated from two equations, that is Equation (16) and

$$\Delta h = 1.5 \left(\frac{v^2 d^2 T_a}{4 T_s u_h} \right)^{1/3} \quad (20)$$

where all parameters are defined as before. The lower of the two stable momentum rises is then compared to the lower stable buoyant rise and the higher of those two is taken for the final plume rise for stable air.

5.3 AERMOD Dispersion Model

AERMOD software for atmospheric dispersion modeling, with the commercial interface AERMOD View, version 8.2 (Lakes Environmental Software, Canada) was used to predict the H_2S concentrations in the vicinity of San Jacinto-Tizate geothermal power plant for different time periods. The model description and data needed to run the model is depicted below.

5.3.1 Model Description

The American Meteorology Society-Environmental Protection Agency developed AERMOD model, a software package based on Gaussian plume equation. It is the recommended model by the U.S EPA for air quality simulations.

AERMOD is a steady-state plume model designed to estimate the near-field (less than 50 km) concentration and run with a minimum of observed meteorological parameters. In the stable boundary layer (SBL), it assumes the concentration distribution to be Gaussian in both the vertical and horizontal. In the convective boundary layer (CBL), the horizontal distribution is also assumed to be Gaussian, but the vertical distribution is described with a bi-Gaussian probability density function (pdf). It treats both surface and elevated sources on simple and complex terrain. Special features in AERMOD include its ability to treat the vertical heterogeneity of the planetary boundary layer, special treatment of surface releases, irregularly-shaped area sources and the limitation of vertical mixing in the stable boundary layer (Cimorelli *et al.*, 2004).

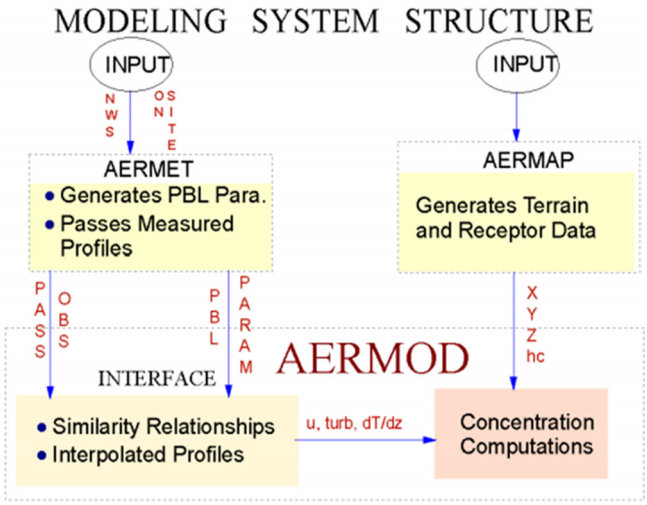

Figure 5-4. Data flow in the AERMOD modeling system (Cimorelli et al., 2004).

AERMOD input data is prepared from output files from AERMET and AERMAP pre-processors (Figure 5-4). AERMET uses meteorological data and surface characteristics to calculate boundary layer parameters (e.g. mixing height, friction velocity, etc.) needed by

AERMOD. This data, whether measured off-site or on-site, must be representative of the meteorology in the modeling domain (Cimorelli *et al.*, 2004).

AERMAP uses gridded terrain data for the modeling area to calculate a representative terrain-influence height associated with each receptor location. The gridded data is supplied to AERMAP in the format of a Digital Elevation Model (DEM), from which elevations for both discrete receptors and receptor grids are computed. AERMAP provides information that allows the dispersion model to simulate the effects of air flowing over hills or splitting to flow around hills; providing a physical relationship between terrain features and the behavior of air pollution plumes.

Surface characteristics in the form of albedo, surface roughness and Bowen ratio, plus standard meteorological observations (wind speed, wind direction, temperature, and cloud cover), are input to AERMET. AERMET then calculates the PBL parameters: friction velocity, Monin-Obukhov length, convective velocity scale, temperature scale, mixing height, and surface heat flux. These parameters are then passed to the INTERFACE (which is within AERMOD) where similarity expressions (in conjunction with measurements) are used to calculate vertical profiles of wind speed, lateral and vertical turbulent fluctuations, potential temperature gradient, and potential temperature (Cimorelli *et al.*, 2004).

5.3.2 Input Data

Source Data

The H_2S emissions from San Jacinto-Tizate geothermal power plant are made through the cooling towers. When the power plant operates at full load, these are modeled as two stacks with the characteristics shown in Table 5-5.

Table 5-5. Source input data for AERMOD.

SJT Power Plant (72 MW)		Coordinates*	X	Y
Base elevation (m.a.s.l.)	185			
Release Height (m)	14	Stack 1	524516.17	1393922.64
Stack inside diameter (m)	24.6			
Gas exit velocity (m/s)	3	Stack 2	524599.22	1393931.39
Gas exit temperature (°C)	40			
Emission rate (g/s)	45.5			

*Coordinates UTM, Zone 16 Northern Hemisphere

Meteorological data

Time series of weather parameters (hourly surface observations) were input to AERMET meteorological pre-processor, which organize the available meteorological data into a format suitable for AERMOD. Upper air data (vertical temperature gradient and wind profile) was computed by the upper air estimator within AERMET, based on hourly surface data.

AERMET calculates atmospheric parameters needed by AERMOD dispersion model, such as atmospheric turbulence characteristics, mixing heights, friction velocity and sensible heat flux. The standard meteorological data pre-processing accounts for site specific

parameters such as land surface characteristics (albedo, surface roughness, Bowen ratio) within a 3 km radius around the weather station where the surface observations are made.

For this, the land cover classification was made based on three sources of data:

- Google earth satellite imagery.
- Land use maps from the project' Environmental Impact Assessment.
- Topographic map (Scale 1:5000) provided by INETER.

The surface parameter coefficients (albedo, Bowen ratio and surface roughness) for AERMET meteorological pre-processor were set to summer conditions for both wet and dry season model simulations of the climate in Nicaragua. This was considered to represent the closest analogue for seasonal conditions in the US and Canada, where the model was developed.

Variable surface roughness parameters were used based on the land cover around the SJT weather station. The Wieringa- Davenport roughness classification (Wieringa, 1992) was used as reference for selecting the values to use within AERMET options. Given the different land use in the area, the classifications used were "Roughly open" (z_0 = 0.1 m) for cultivated areas with low crops or plant covers, "Rough" (z_0 = 0.2 m) for cultivated areas with crops of varying heights and "Very Rough" for areas with clumps of trees and bush land (z_0 = 0.8 m).

Finally, AERMET creates two files for AERMOD: a surface file of hourly boundary layer parameter estimates and a profile file of multiple-level observations of wind speed and direction, temperature, and standard deviation of the fluctuating components of the wind.

Terrain data

Terrain is one of the factors that affect air pollution where atmospheric vertical motion due to low or high pressure system or complex terrain effect and elevation above the ground (Zannetti, 1990). The presence of elevated terrain can significantly affect ground level concentrations of air pollutants emitted from elevated sources, by reducing the distance between the plume centerline and ground level and increasing turbulence and funneling of plumes around topographical features.

AERMAP terrain pre-processor uses gridded terrain data to calculate a representative terrain-influence height and assigning elevation data to each receptor. This is input to AERMOD to handle the computation of pollutant impacts in both flat and elevated terrain. A digital elevation model (DEM) with a resolution of 30 m of posting interval and 7-14 m accuracy was downloaded from ASTER GDEM website, data provided by METI/NASA. The DEM was directly input to AERMAP and considering the topography in the project area, the flat and elevated option was chosen when running AERMOD dispersion model.

Buildings

AERMOD incorporates the effects of buildings in the plume growth and plume rise. For sources influenced by a building, the plume rise is estimated using a numerical model that includes effects from streamline deflection near the building, vertical wind speed shear, enhanced dilution from the turbulent wake and velocity deficit. In general, these building

induced effects act to restrict the rise that the plume would have in the absence of the building (Cimorelli *et al.*, 2004).

The movement of air over and around buildings generates areas of flow circulation, which can lead to increased ground level concentrations in the building wakes. Downwash effects can be significant, where building heights are greater than about 30 - 40% of the stack height (RPS, 2009), and distance less than 1 km from the emission source (Zannetti, 1990).

In the San Jacinto-Tizate project area, the only buildings likely to affect dispersion are the power house and the cooling towers' own structure. Rectangular buildings were selected to represent the layout of the power plant (Figure 5-5). The location and dimension of the buildings was input to AERMOD to incorporate the buildings downwash effect in the modeling results. The dimension (*L, W, H*) of the cooling towers used in the model was 74.7 x 18.7 x 12 m and 77.8 x 32 x 16 m for the power house building.

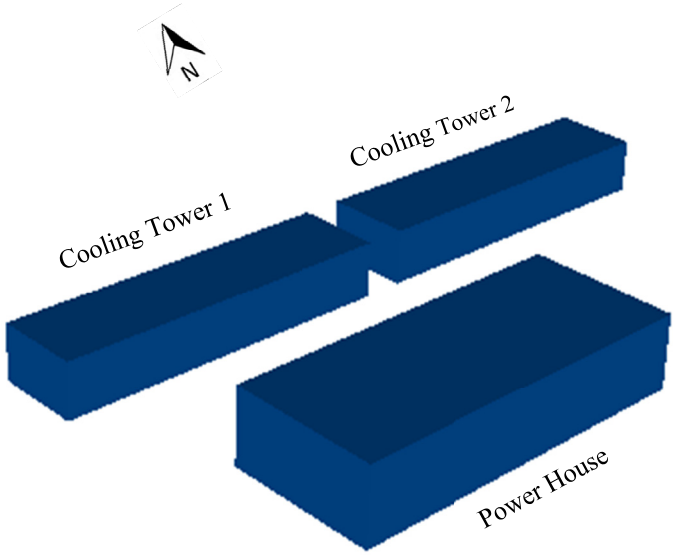

Figure 5-5. San Jacinto-Tizate power plant layout in the model.

Receptors

Discrete Cartesian receptors and uniform Cartesian grids were defined within the modeling domain to identify areas of maximum predicted H_2S concentrations. The location of populated areas in the vicinity of San-Jacinto Tizate power plant was carried out through a review of satellite imagery from Google Earth and a topographic map (scale 1:5000) from the study area.

Within the discrete receptors, control points were defined in agreement with points from the air quality monitoring program implemented by PENSA. Additional receptors were located in populated areas in the surrounding villages.

Different grid sizes were used to provide a good resolution of predicted concentrations near the power plant area (where concentrations can vary greatly over a smaller distance), as well as for covering a wider area from the source (modeling domain). The following grid sizes and resolutions were used together:

- Grid 1: 30 x 30 km with 1000 m grid spacing
- Grid 2: 5 x 5 km with 300 m grid spacing; and
- Grid 3: 1.5 x 1.5 km with 50 m grid spacing

5.3.3 Modeled Periods

Three different short periods were modeled in AERMOD, in agreement with air quality monitoring dates. The input data was adjusted to different power plant operation conditions for the specific dates (Table 5-6). The last modeled period represents the power plant operating at full load for a whole year, using meteorological data from January to December 2012.

Table 5-6. Input data for the modeled periods.

SJT Power Plant	March 6 - 7 2012	September 19 - 20 2012	June 6 - 7 2013	Full year
Electricity generation (MW)	39	38	59	72
Emission rate (g/s)	24.7	24.1	37.3	45.5
Gas exit velocity (m/s)	3	3	3	3
Number of stacks	1	1	2	2

6 Modeling Results

6.1 Simple Gaussian Plume Estimates

A simple Gaussian plume approach was used to analyze the change in concentrations with distance from the source. Three different periods were modeled according to the weather conditions for each specific date (6 - 7 March 2012, 19 - 20 September 2012 and 6 - 7 June 2013) and the H_2S concentration at ground level considering different atmospheric stability was computed. The emission rate used was that of the power plant operating at full load for all periods (45.5 g/s).

The atmospheric stability was classified as shown in Section 5.2.2. For atmospheric stabilities *A* and *B* (more unstable), an air temperature of 32°C and a wind speed of 1 m/s and 3 m/s was used in the model. For *C* and *D* (slightly unstable and neutral) stabilities, the wind speed used was 7 m/s and an air temperature of 30 °C and 28°C respectively. During stabilities *E* and *F* (more stable), the air temperature used was 25°C and wind speeds of 2 m/s and 3 m/s, respectively. Wind direction is assumed to be constant.

In 6 - 7 March 2012 (dry season) the atmospheric stability class changed from neutral (*D*) to slightly unstable (*C*), slightly stable (*E*) and stable atmosphere (*F*). The plume travels farther away during stable conditions, indicating very low concentrations close to the source at night-time and reaching the maximum ground level concentration some 8 km from the source (Figure 6-1). During neutral and slightly unstable atmospheric conditions (day time), higher ground level concentrations are expected closer to the source, with maximum concentrations occurring within a distance about 2-4 km.

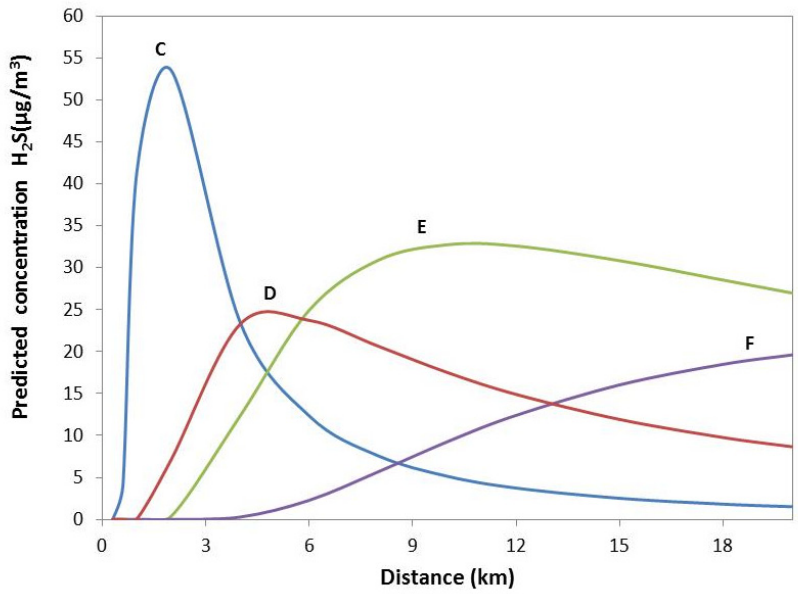

Figure 6-1. H_2S concentration as a function of distance from the source for the atmospheric stability classes occurring on 6 - 7 March 2012.

The months of September and June correspond to wet season in Nicaragua. The atmospheric stability for the periods 19 - 20 September 2012 and 6 - 7 June 2013 was very similar. The atmospheric stability class changed from extremely unstable (*A*) to moderately unstable (*B*), slightly stable (*E*) and stable atmosphere (*F*). The plume travelled farther away during stable conditions, indicating very low concentrations close to the source at night-time and reaching the maximum concentration at a distance greater than 8 km from the source. During extremely unstable and moderately unstable conditions (day time), the maximum concentrations occur about 1-2 km from the source for both months (Figure 6-2).

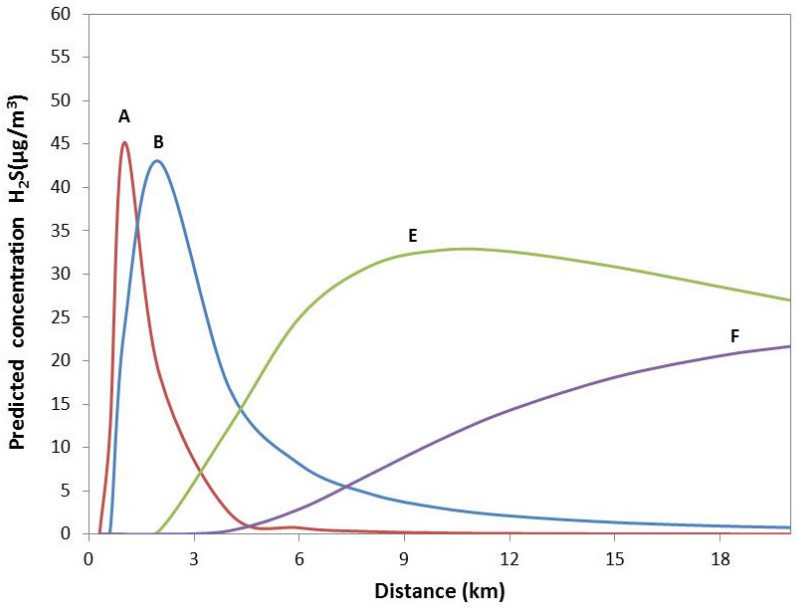

Figure 6-2. H_2S concentration as a function of distance from the source for the atmospheric stability classes occurring on 19 - 20 September 2012 and 6 - 7 June 2013.

6.2 AERMOD Model Results

Four different periods were modeled in AERMOD. The first one considering the San Jacinto-Tizate power plant operating at full load (72 MW) for a whole year, using meteorological data from the period January-December 2012. The other three periods were modeled in agreement with the H_2S monitoring periods by PENSA in March and September 2012 and June 2013.

6.2.1 Power Plant Operating at Full Load (72 MW)

Different time averaging options were considered to analyze the spatial distribution of the plume and H_2S ground level concentrations in the study area. The annual average and three short term maximum average concentration (1h, 8 h and 24 h) during the year 2012 were chosen to study the distribution of hydrogen sulfide. Lastly, the number of times that the WHO ambient air guideline for H_2S (150 µg/m^3 averaged over 24 h) and the guideline value set in Iceland (50 µg/m^3 averaged over 24 h) are exceeded during the modeled period is presented.

Annual Average

The San Jacinto-Tizate power plant operating at full load for a whole year was modeled. In AERMOD modeling software, the long-term averages do not include calm or missing hours in their calculations. The annual average is simply the sum of the concentrations from the non-calm/non-missing hours divided by the number of non-calm/non-missing hours.

The modeling showed that the highest concentrations are to be expected in the immediate vicinity of the power plant (Figure 6-3).The maximum concentration predicted was 116µg/m^3 and occurs next to the power plant building. The San Jacinto village and other smaller settlements are located outside of the plume pathway, except for few isolated dwellings or farms located in the places identified as Receptor A, Los Prados and El Ojochal del Listón (Figure 6-3).

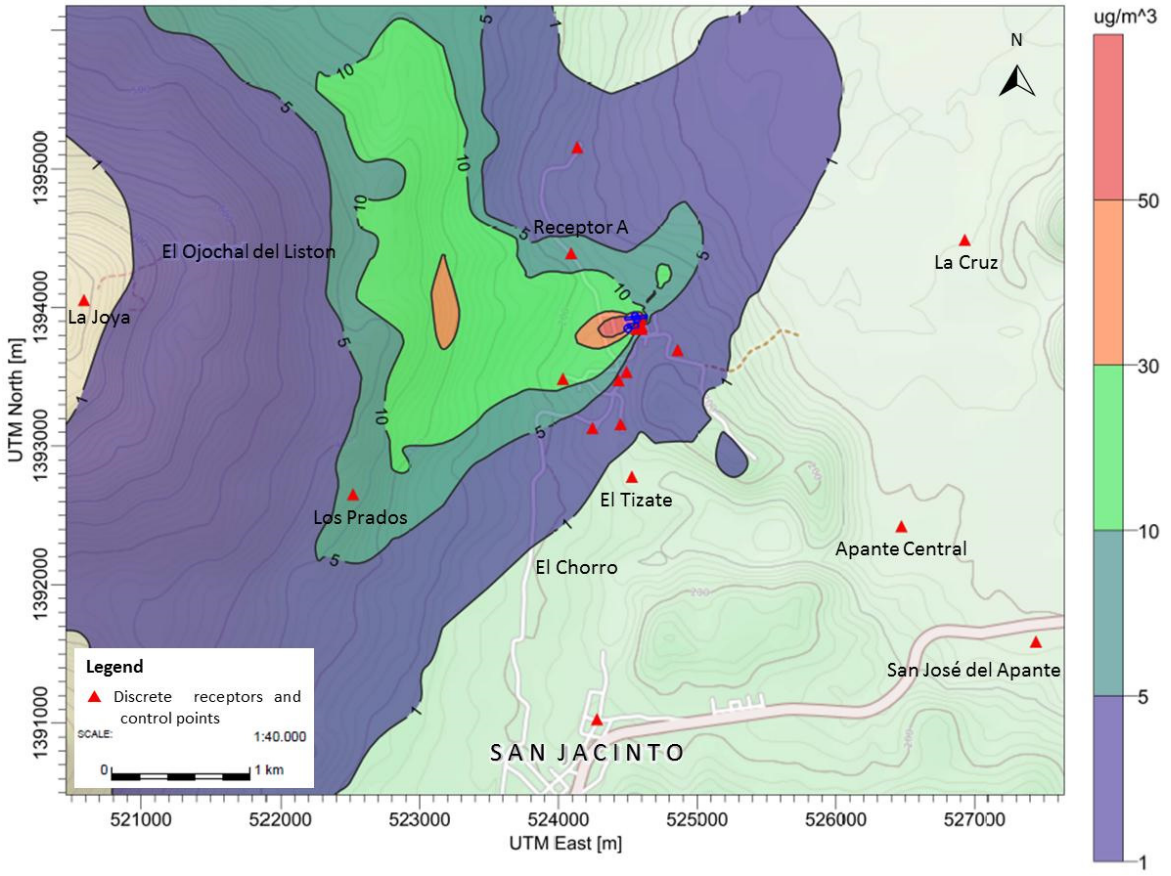

Figure 6-3. Annual average H_2S concentration for the modeled conditions in 2012.

Highest 24-hour average

The short term average results from AERMOD represent the highest concentrations reported by receptor for the averaging period. The contours are based in the highest 24h average concentration by receptor, occurring at different times for different locations (Figure 6-4).

The spatial distribution of the plume for 24h averaging time extends over a wider area than the annual average, including populated places, where H_2S concentrations up to 50 µg/m^3 are predicted (Figure 6-4). The highest concentration occurs about 1.2 km west from the source, and also near the power plant building, where a peak value of 1462 µg/m^3 is predicted on 7 March 2012. In these places, the WHO ambient air guideline of 150 µg/m^3 averaged over 24 h is greatly exceeded.

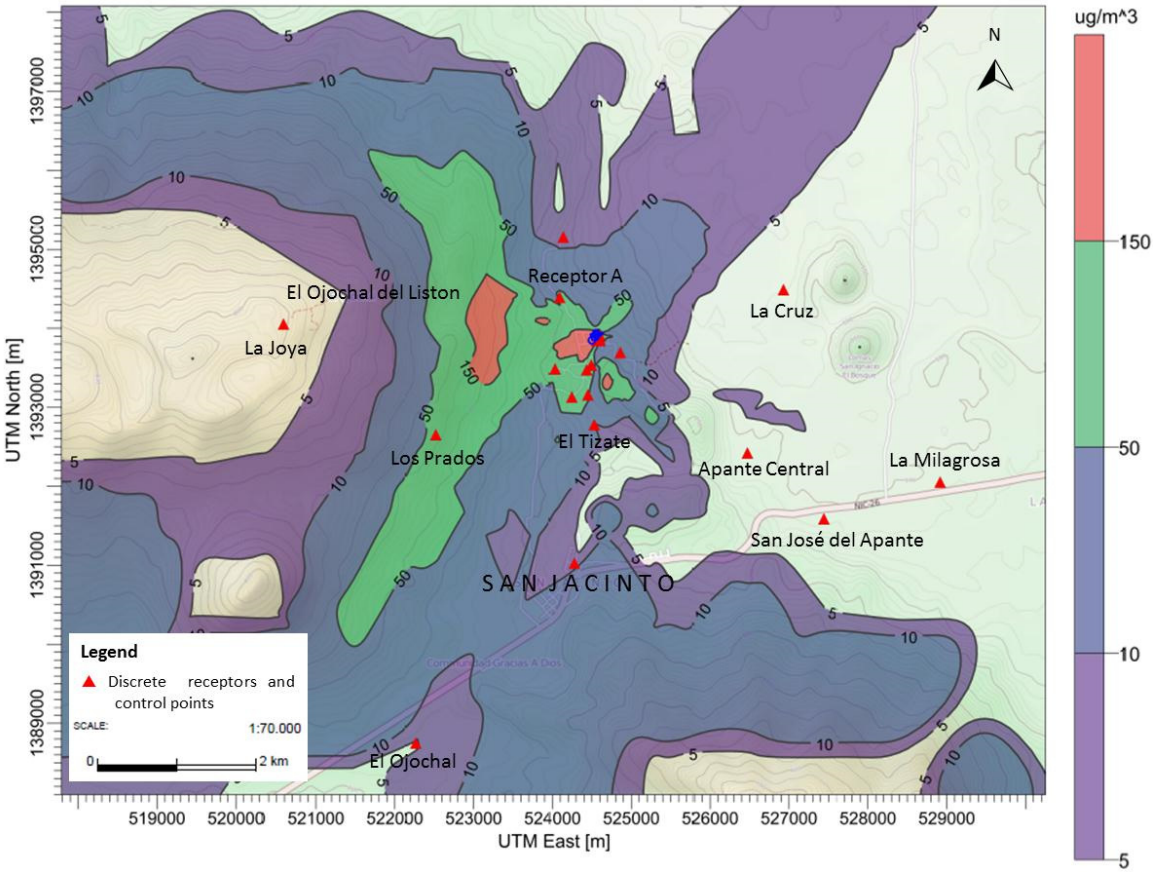

Figure 6-4. Highest H_2S 24 hour average concentration at any given location for the modeled year 2012.

Highest 8-hour average

The highest concentration in an 8 hour averaging time was also modeled. The results show that the concentration can reach really high levels in the immediate vicinity of the power plant, reporting a peak value of 2382 µg/m^3 on 7 March, 2012 from 16:00-00:00, located in between the Power House building and the Cooling Tower 1 structure (Figure 6-5). In most of the populated places the H_2S concentration range from 10-150 µg/m^3. The 8 h average concentration is mainly used for occupational safety purposes, where the exposure limit may vary from 7100 - 14200 µg/m^3 (European Commission and ACGIH respectively). None of these exposure limits for 8-hour averaging period is exceeded in the study area.

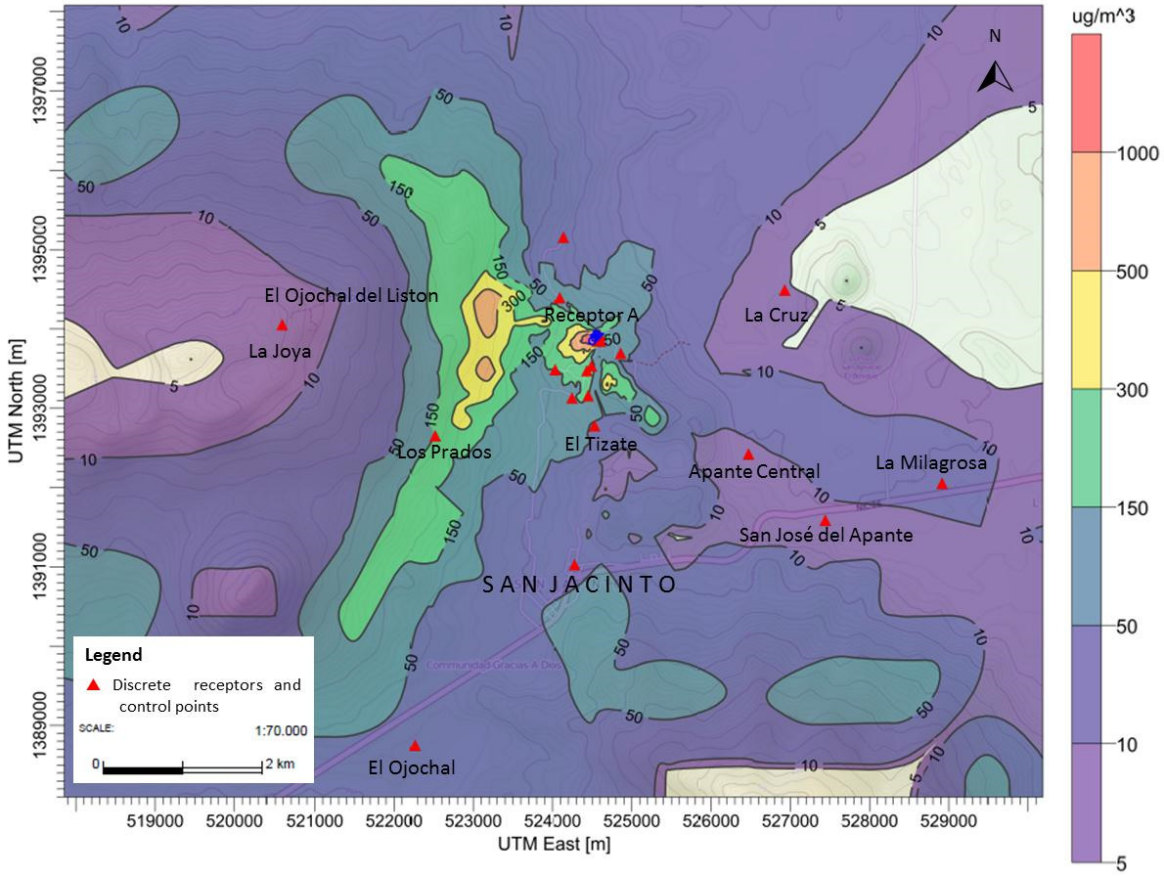

Figure 6-5. Highest H_2S 8 hour average concentration at any given location for the modeled year 2012.

Highest 1-hour average

This represents the shortest averaging time that can be modeled in AERMOD. For a one hour average, only a single hour with the highest concentration during the modeled year is taken by receptor to build the concentration contours (Figure 6-6). The results do not represent a snapshot in time, as the highest values occur at different times for different locations. A peak concentration value of 2871 µg/m^3 is predicted on 8 March 2013 at 13:00, occurring in between the power house building and Cooling Tower 1 structure.

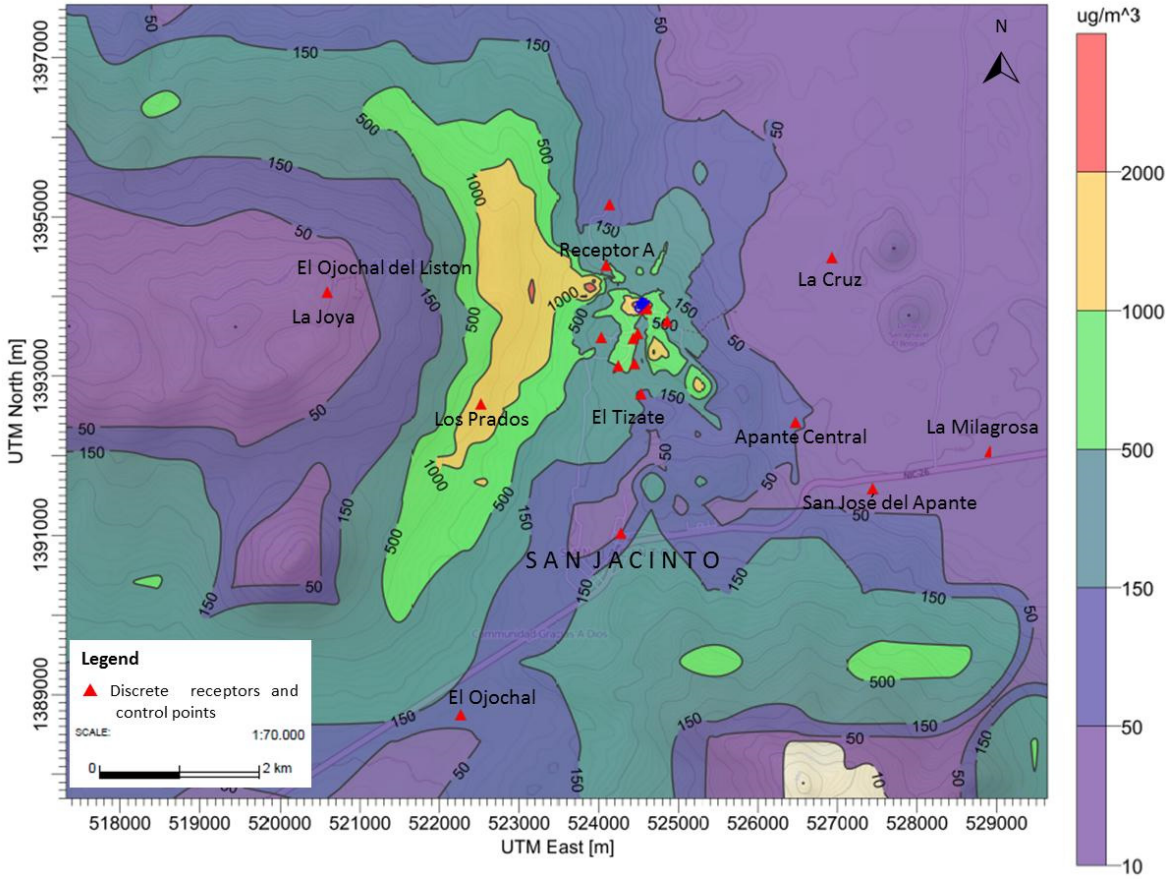

Figure 6-6. Highest H_2S 1 hour average concentration at any given location for the modeled year 2012.

The location of maximum concentrations for all the modeled averaging periods occurs at the same site, the west sector from the power plant site. This result is in agreement with the prevailing ENE and E winds in the San Jacinto-Tizate project area.

The peak concentration values occurred in between the Cooling Tower 1 structure and the Power House building for all averaging times. This can be associated to building downwash effects, since the movement of air over and around buildings generates areas of flow circulation, which can lead to high ground level concentrations in the building wakes (RPS, 2009).

Ambient Air Threshold Violation Predictions

The number of times that the WHO ambient air guideline for H_2S (150 µg/m^3 averaged over 24 h) is exceeded in a year was also obtained from the modeling in AERMOD. It can be noticed in Figure 6-7 that the WHO guideline value is exceeded at least 1-5 times within a distance about 1 km from the power plant in the W, WNW and WSW direction. In the immediate vicinity of the power plant the value is exceeded numerous times, predicting up to 77 times in a year next to the exhaust from the cooling towers.

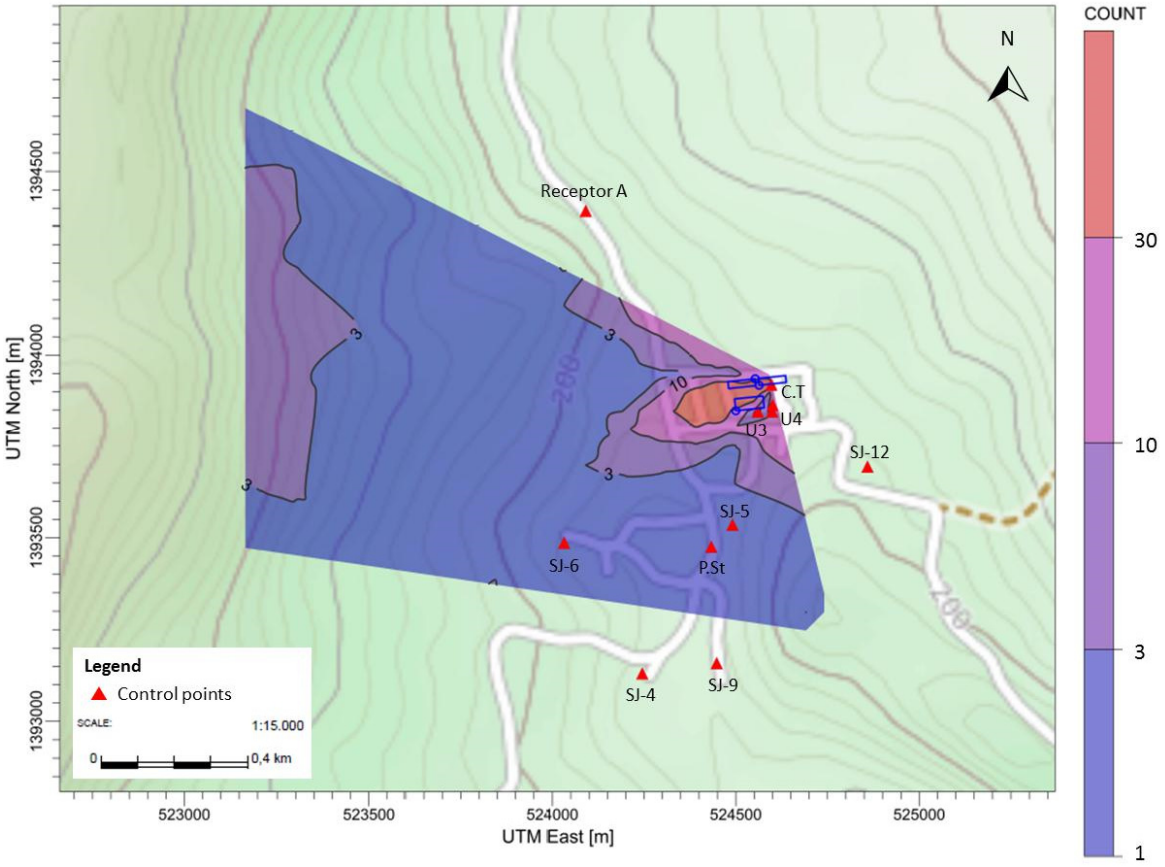

Figure 6-7. Number of times the WHO guideline for H_2S is exceeded in a year.

In order to better assess the environmental effect of H_2S emissions on air quality in the surrounds of the San Jacinto-Tizate geothermal power plant, the ambient air guideline set for H_2S in Iceland (50 µg/m^3 averaged over 24 h) was also used for analyzing the threshold violation predictions. This guideline value is given for the same time averaging indicated by the WHO guidelines (24 hours).

The result shows that the H_2S ambient air guideline set in Iceland is exceeded at least 2-10 times a year within a distance about 2.5 km west from the power plant (Figure 6-8), however, no populated places were identified within the threshold violation area. Near the power plant the value is highly exceeded, predicting up to 166 times in a year close to the exhaust from the cooling towers.

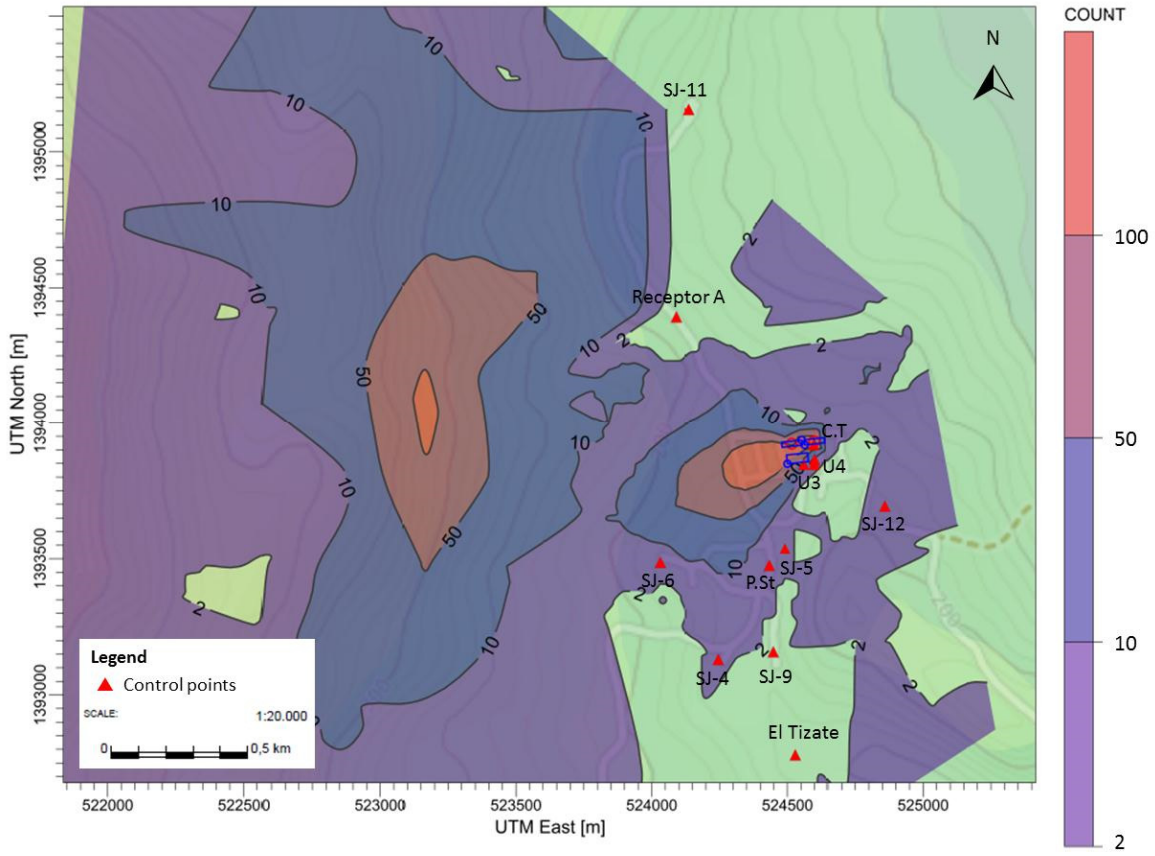

Figure 6-8. Number of times the H_2S guideline value used in Iceland is exceeded in a year.

6.2.2 The Period 6 – 7 March 2012

This period was modeled for comparison purposes with averaged H_2S concentrations reported by PENSA. The modeling period started on 6 March at 20:00 and ended on 7 March at 19:00, covering the same hours considered in the averaged concentrations. During these days, the average air temperature was 28 ± 2°C and the average wind speed was 7 ± 3 m/s. The prevailing wind direction was ENE (55 % of the time) and NE (33%).

The same coordinates and monitoring points set by PENSA were used for predicting the average concentration at ground level: Receptor A, El Tizate, SJ-12, SJ-11, SJ-9, SJ-6, SJ-5, SJ-4, Cooling Tower (C.T), Pumping station (P.St), Power Plant Unit 1 and 2 (U1-2) and Power Plant Unit 3 (U3). The spatial distribution of the plume was identified in SW direction (Figure 6-9), in agreement with prevailing ENE and NE winds for these days. Very few monitoring points were found within the plume during the modeled period, these are SJ-6, C.T and U1-2. The maximum concentration was predicted near the power plant site.

When comparing the predicted averaged concentrations from modeling with the reported averaged concentration, it was found that AERMOD underestimated the concentration in all the control points (Figure 6-10). Considering that the reported concentrations for the period under study correspond to the highest values reported in the project area in 2012, a review of the possible reasons for the discrepancy in predicted concentrations by the model was done.

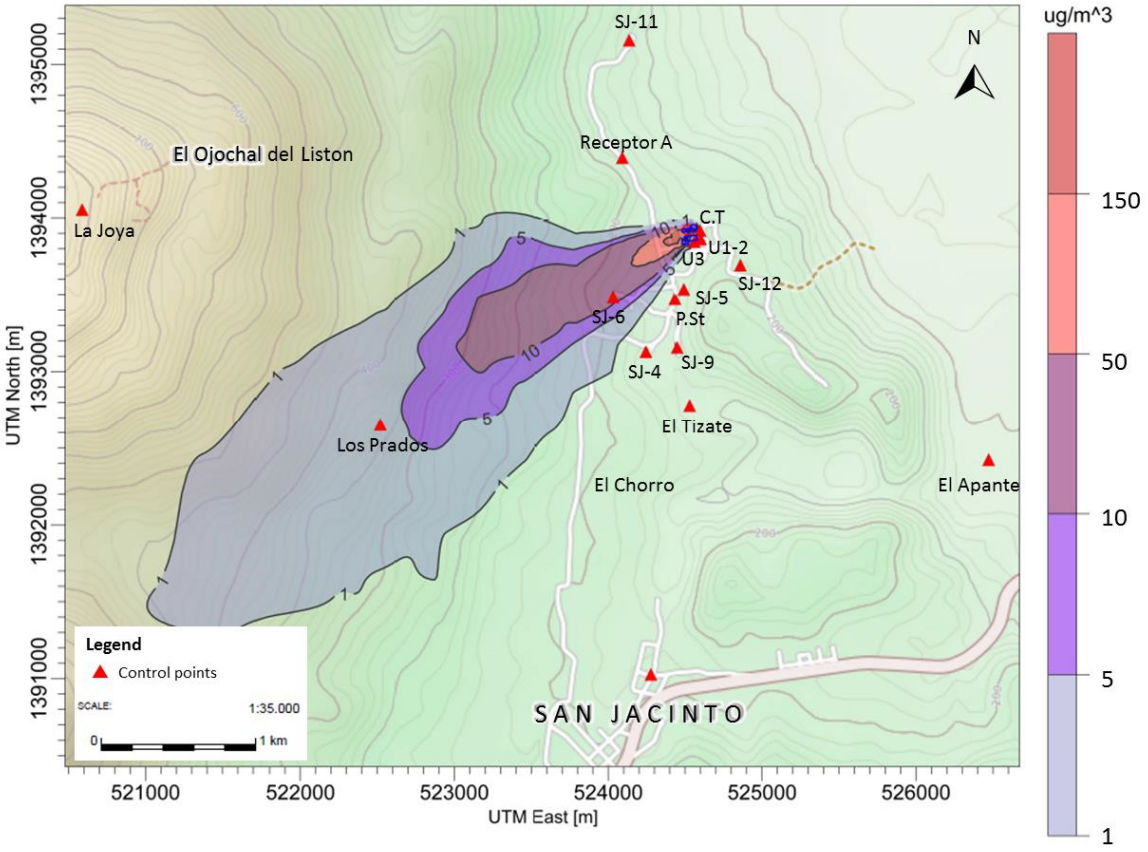

Figure 6-9. Predicted H_2S average concentration for 6 - 7 March 2012.

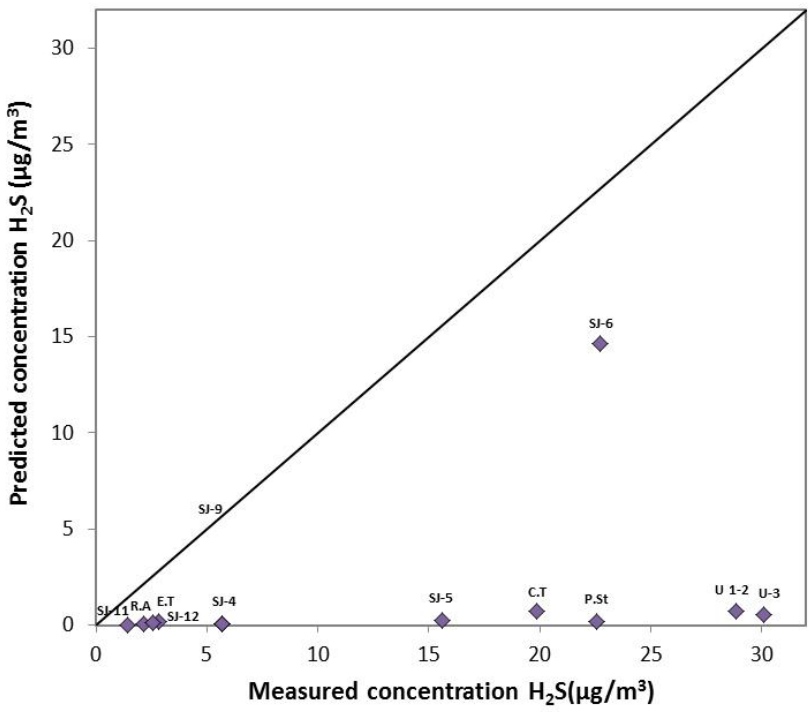

Figure 6-10. Relation of measured and predicted H_2S concentrations on 6 - 7 March 2012.

Based on a review of the electricity generation for the period, it was found that the San Jacinto-Tizate power plant was not operating normally, reporting highly variable electricity generation for some hours due to power plant restrictions. The daily generation reports from the National Load Dispatch Center (CNDC by its Spanish acronym) available in the online database were reviewed, finding that during the H_2S monitoring period, the old backpressure power plant (Unit 1-2) was operated for some hours and the condensing power plant (Unit 3) had some operational restrictions (Figure 6-11). The backpressure power plant consist of a different technology (lower efficiency or higher steam consumption), discharging all the steam and non-condensable gases directly from the turbine exhaust at atmospheric pressure, meaning a different emission rate, much higher exit temperature (~ 100°C) and velocity and very close to the ground (~ 4 m). When the emissions are made close to the ground, like in this case, higher H_2S ground level concentrations are to be expected. In addition, when the condensing unit had operational problems, the steam in the production pipeline is discharged through a rock muffler close to the power plant and other times through the silencers in the production wells, which emissions characteristics are similar to the backpressure power plant.

The above mentioned situations in the power plant operation may have caused very unstable atmospheric conditions and increased mixing with the surrounding air, which can lead to increased ground level concentrations close to the source. The measured H_2S concentrations during the monitoring period may have captured some of the changes previously discussed, although no details of power plant specific operation conditions or individual measurements are presented in the H_2S monitoring reports.

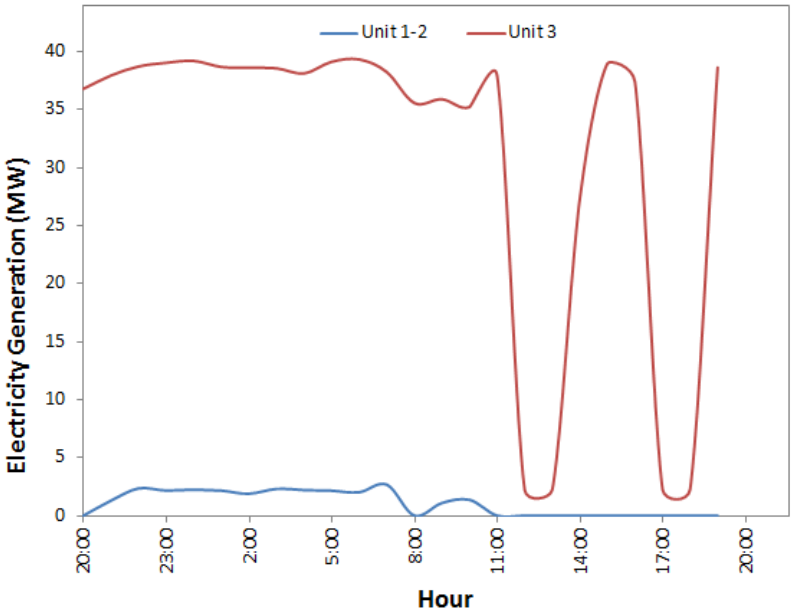

Figure 6-11. Electricity generation on 6 - 7 March 2012 (data from CNDC).

6.2.3 The Period 19 - 20 September 2012

The modeled period started on 19 September at 13:00 and ended on 20 September at 14:00, covering the same hours considered in the reported averaged concentrations. The monitoring points for this period were the same as in March 2012, except that Power Plant

Unit 1 and 2 (U1-2) is no longer included. During the modeled period, the average air temperature was 28 ± 3°C and the average wind speed was 2 ± 1 m/s, with prevailing ESE (19 % of the time), E (18%) and SSE (15%) winds.

The majority of the H_2S monitoring points were located outside of the predicted plume pathway for the modeled period, as shown in Figure 6-12. The maximum concentration occurred some 1.3 km NW from the power plant.

When comparing the measured average concentration with predicted concentrations, the model underestimated the measurements in the majority of the monitoring points, except for Receptor A, where the predicted concentration was slightly higher (Figure 6-13). In the case of the Pumping station (P.St), the high measured concentration may not be associated to the power plant emissions but to the specific characteristics of the point location. This site lies next to the separated water pond (brine) and very close to fumaroles in the surrounding area, which natural H_2S emissions might be captured by the measurements in every monitoring period.

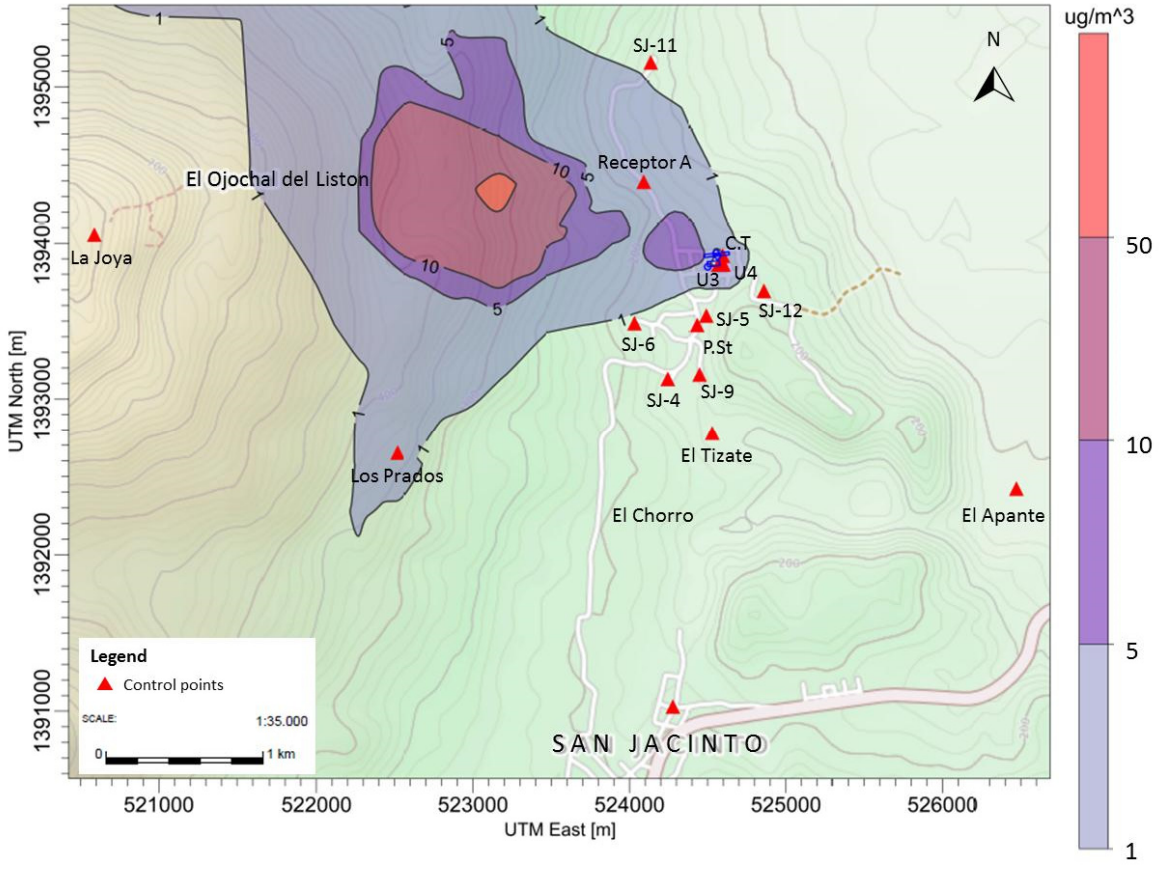

Figure 6-12. Predicted H_2S average concentration for 19-20 September 2012.

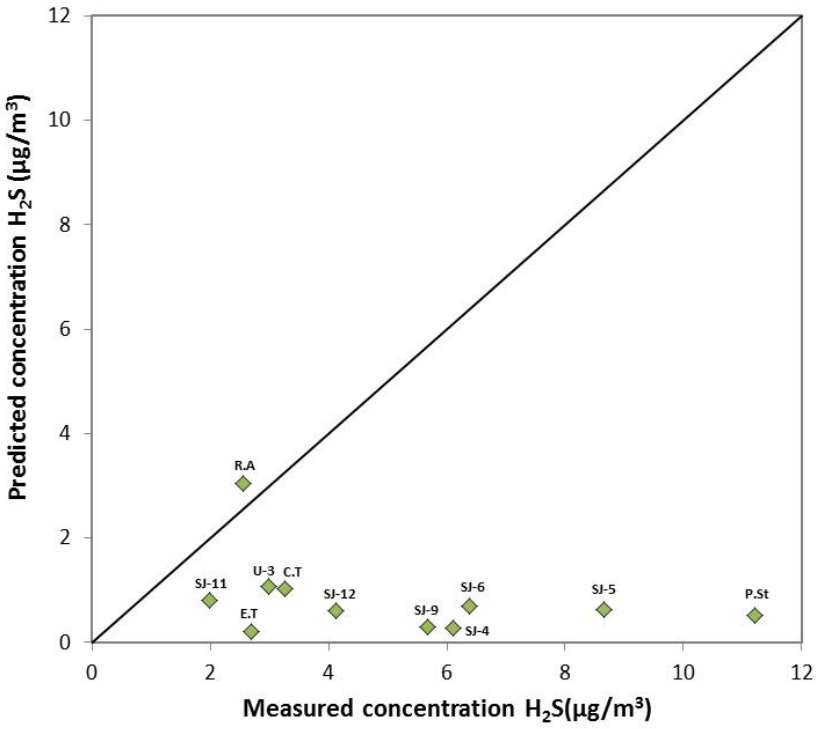

Figure 6-13. Relation of measured and predicted H_2S concentrations on 19-20 September 2012.

6.2.4 The Period 6 - 7 June 2013

The modeled period started on 19 June at 15:00 and ended on 20 June at 14:00, covering the same hours considered in the reported averaged concentrations. The monitoring points for this period were the same as in September 2012, except that a point for the Power Plant Unit 4 (U4) was added. In the modeled period, the average air temperature was 27 ± 3°C and the average wind speed was 2 ± 1 m/s, with prevailing SSW (29 % of the time), SSE (21%) and SW (14%) winds.

During this period, many of the H_2S monitoring points were located within the plume (Figure 6-14), with maximum concentrations occurring some 0.3 km WNW from the power plant. The comparison of the measured and predicted averaged concentrations showed that some points were fairly predicted (Cooling Tower, Power plant Unit 3 and Unit 4) while others (Receptor A and SJ-11) were largely overestimated by the model. The rest of the monitoring points were underestimated, as happened with other modeled periods (Figure 6-15).

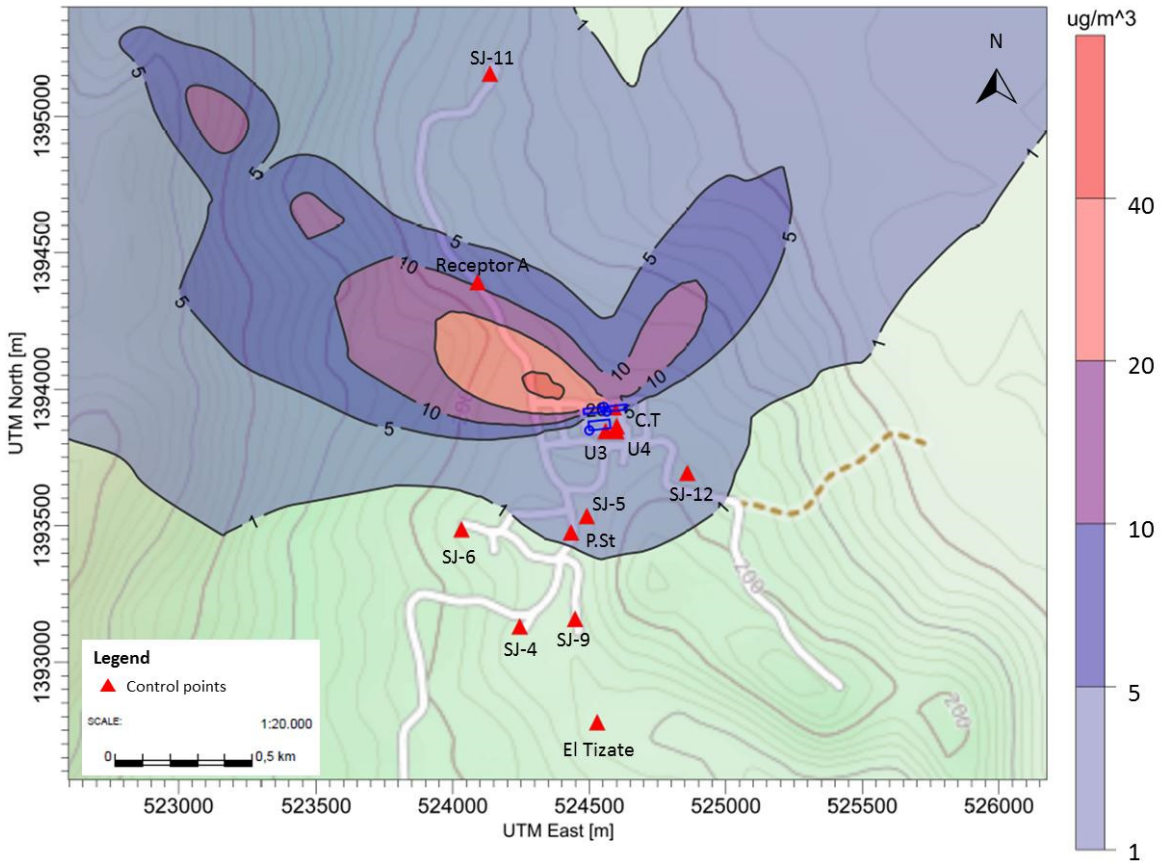

Figure 6-14. Predicted H_2S average concentration for 6 - 7 June 2013.

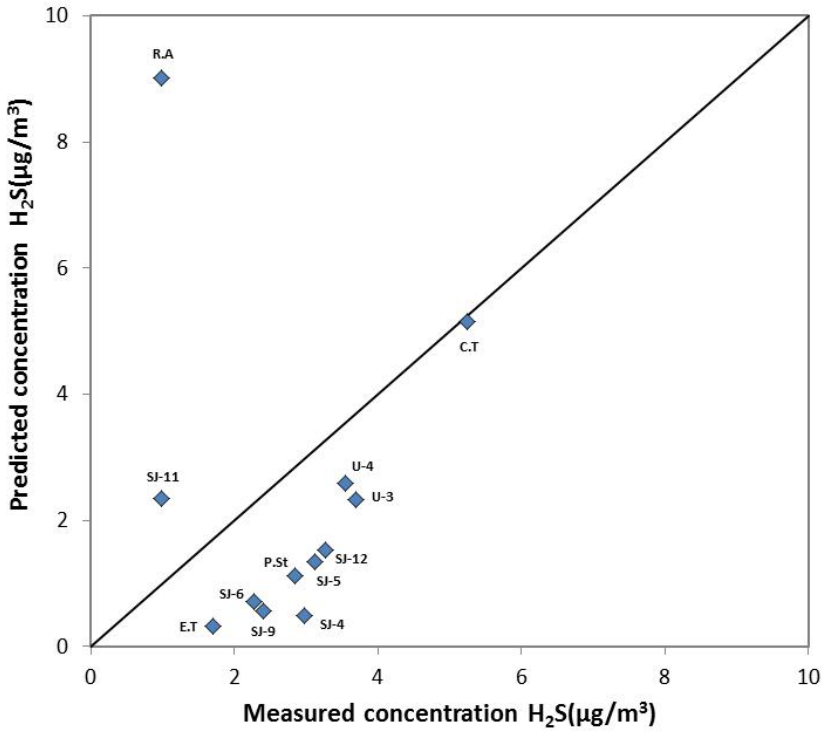

Figure 6-15. Relation of measured and predicted H_2S concentrations on 6 - 7 June 2013.

7 Discussion

The results from modeling show that the operation of the San Jacinto-Tizate geothermal power plant does not significantly affect the air quality of the neighboring communities. Populated places are located outside the prevailing plume pathway during the modeled periods.

Understanding the atmospheric stability according to different weather conditions and time of the day is very important for the proper interpretation of dispersion modeling results. During stable conditions, high concentrations of a pollutant can be expected farther away from the emitting source and very low close to it (Figure 6-2). On the other hand, during unstable conditions higher concentrations may occur very close to the source as a result from turbulence caused by rapid overturning of air (USEPA, 2005).

When modeling the San Jacinto-Tizate geothermal power plant operating at full load for a whole year, using weather data from 2012, AERMOD model shows that H_2S emissions mostly affects the air quality in the immediate vicinity of the project. The plume centerline was oriented towards W, spreading to NW and SW most of the time, in agreement with prevailing ENE and E winds in the area. The surrounding villages are located outside of the most common plume pathway the majority of the time, however when modeling short averaging times (1h and 8h) over a whole year, concentrations in the range of 50 -150 $\mu g/m^3$ are predicted at some populated places.

The WHO ambient air guideline value for H_2S (150 $\mu g/m^3$ averaged over 24 h) is only exceeded within 1.2 km distance from the power plant in the west direction. Nevertheless, the occupational safety guidelines (7000-14200 $\mu g/m^3$ averaged over 8 h) are never exceeded at any location in the study area.

When comparing the results form AERMOD model with measured averaged concentrations in the periods 6-7 March 1012, 19-20 September 2012 and 6-7 June 2013, the model predicted very low concentrations for the majority of the points in every modeling period. For two specific points located north from the source (Receptor A and SJ-11), the model predicted much higher concentrations, results that could be associated to the effect of the terrain and surface roughness characteristics of the location, where land cover was classified as grassland. In the case of Receptor A, the high predicted concentrations could be also related to its proximity to a small depression for which high ground level concentrations are also predicted in the west side of the power plant site.

Natural release of H_2S from fumaroles in the project area is not accounted for in modeling, however these natural sources can affect the measured concentrations used for comparison with the model results. In one of the three periods for which H_2S measurements were available (6-7 March 2012), the source input parameters used in the model did not apply to the power plant conditions, given the operation of the backpressure power plant for some hours and the unstable operation of the condensing power plant throughout the monitoring period.

The accuracy of the location of some of the monitoring points may also affect the concentrations values predicted by AERMOD. For example in the power plant area, the measurements reported to be taken in the Unit 3 (west sector from the power house building) and in the cooling tower, seems to be shifted to the East by some meters, affecting its location within the proper concentration contours calculated by the model. However for the location of the control points in the modeling domain, the same coordinates reported by PENSA for the concentration measurements were used.

The modeling predictions showed a better agreement with measured concentrations when the monitoring points were located closer to the plume centerline whereas the agreement was generally very poor for points located near the plume edge. However it should be mentioned that the fair prediction of some of the measured values at some monitoring points indicates that assumptions made to constrain the H_2S concentration as well as other source characteristics like emission temperature and velocity are not completely off from real values but in a range of divergence.

Sensitivity analysis was conducted on two source input parameters, the gas exit velocity and rate of gas release from the power plant, the latter based on two possible conditions that could control the H_2S concentration in the geothermal system. If the concentration of H_2S in the geothermal reservoir was controlled by the more reducing reaction **a** instead of reaction **b**, the predicted concentrations at ground level will increase by a constant factor (linear increase) at each receptor or monitoring point considered, predicting 64% higher values. This however is unlikely to occur in the San Jacinto-Tizate geothermal reservoir, because the mineral assemblages considered in reaction **a** represent highly reduced conditions in a geothermal system, a condition that has not been reported for this geothermal field.

When reducing the gas exit velocity from 3 m/s to 2 m/s the predicted concentrations increased by variable factors, depending of the location of the specific monitoring points. In the case of points located very close to the source, the predicted concentration increased up to 200% while for points located further away the concentration increase is about 20-40%.

To provide a better analysis of the relevance of the model prediction in relation to measured concentrations, some adjustment in the input data should be made in accordance to the real operation conditions in the power plant, meaning the use of measured H_2S concentration in the steam and the air flow in the cooling towers to compute the exact gas exit velocity. In addition, increasing the number of monitoring points to cover a wider area in the west direction from the source could provide better background data for comparison with the modeling results. The actual measurements are made at locations aligned to the north and south from the source, without providing a wider spatial distribution to account for some spreading of the plume.

The concentration contours obtained from modeling are certainly a useful visualization tool. It has to be underlined; however, that a model is a simplification of a complex process in which many factors interact and therefore the results are approximations that may not accurately reproduce or fit to measured concentrations in a given place.

8 Policy Recommendations

In this section a review of the national policies relevant to air pollutants and emissions from geothermal power plants is made and some recommendations based on the findings of this study are proposed.

In Nicaragua the first air quality policy was passed in 2002, entitled Nicaraguan Mandatory Technical Regulation on Air Quality (NTON 05 012-02). This regulation attempted to improve the air quality in the country by establishing emissions limits for the following air pollutants: particulate matter (PM), carbon monoxide (CO), nitrogen oxides (NO_2), sulfur dioxide (SO_2), ozone (O_3) and lead (Pb). This regulation is basically limited to pollutants related to combustion of fossil fuels from both stationary and mobile sources.

Hydrogen sulfide (H_2S) has not been addressed in any national policy in Nicaragua. While no national guideline is available, project developers are encouraged to follow international standards, usually the World Health Organization guidelines.

The Nicaraguan Environmental Impact Assessment Act (Decree 76-2006), requires all electricity generation projects to obtain an environmental permit from the Ministry of the Environment and Natural Resources (MARENA). The issuance of the permit entails an Environmental Impact Assessment (EIA), in which the environmental effects of a proposed development are documented and the proper management of significant environmental impacts is secured.

An EIA for the San Jacinto-Tizate geothermal project was completed in 2003 and an environmental permit was issued by MARENA. Subsequently, a new EIA was completed for the expansion and technological reconversion of the project to a 72 MW condensing power plant, followed by the issuance of a new environmental permit in 2008 (Administrative Resolution No. 30-2008). The EIA concluded that the main environmental impacts of the project were related to air quality and noise, which could be mitigated through chimneys, silencers, forestry, sound barriers and the use of personal protection equipment by staff (PENSA, 2008).

Air quality monitoring is included in the Environmental Management Plan proposed by the project developer PENSA in the EIA. The environmental permit issued to the San Jacinto-Tizate project includes a clause on the implementation of the proposed plans, where the frequency for the monitoring periods is set at least twice a year during the project operation phase. However, no details about the location of ideal monitoring points or duration of the monitoring periods are stated.

In Nicaragua, the Ministry of Energy and Mines (MEM), the Ministry of the Environment and Natural Resources (MARENA) and the Nicaraguan Energy Institute (INE) are jointly responsible for regulating, supervising and controlling geothermal resource exploration and utilization activities. In the case of geothermal projects, the environmental permits are considered main tool to regulate the operations of the power plants. Reporting of air

monitoring to regulatory bodies and municipalities is also addressed in the environmental permits.

The main weakness identified in the review of the regulation process is related to the design and implementation of the air quality monitoring plans, which is mainly left in the hands of the project developers, without being properly discussed and agreed upon between stakeholders. These plans should be proposed by project developers based on technical and scientific background for locating control points in areas suitable for both monitoring of occupational health and safety and exposure of populated places near the project site. Regulatory bodies should enforce the revision and upgrading of the proposed plans in order to provide more reliable data and a good baseline for decision making.

To date, the H_2S reported concentrations correspond to the average of hourly instantaneous measurements in a 24h period carried out twice a year. The reported concentrations are influenced by the meteorological conditions at the time of the measurements that may or may not represent the predominant H_2S ambient air concentration in the area. It is highly recommended to increase the duration and frequency of the monitoring periods to provide a better time resolution of the H_2S concentration in the project area. The original air monitoring plan proposed by PENSA in the EIA and considered for the issuance of the environmental permit, included the installation of an H_2S monitoring station along with the weather station recently installed in the project area. Compliance of the existing commitments under the environmental permit should be enforced.

The suggested measures are necessary to determine the extent and severity of the hydrogen sulfide emissions and ensure that the public is not exposed to concentrations that may cause a nuisance condition or pose a potential risk to public health. The Ministry of Health (MINSA) should be informed about the ambient air conditions in the area in order to properly document the incidence of diseases that could be associated to changes in air quality. This can provide valuable data for further research.

The energy sector should be encouraged to work in close cooperation with INETER, the institution responsible for operating the meteorological network in the country. These institutions therefore need to develop criterion for defining suitable power plant sites considering the prevailing weather conditions. This will mitigate negative effects on air quality. Energy projects will then be properly planned minimizing potential impacts to nearby communities.

Dispersion modeling could be also used as a tool in the EIA of geothermal projects, which results can be accounted for in the design of the power station structures in order to guarantee enhanced dispersion of the emissions as well as for defining a feasible location of the power plants to avoid further air quality impacts.

Lastly, a very important issue to be address is the lack of publicly available data for research purposes. Project developers should be encouraged to provide sufficient data to regulatory bodies and research institutions to carry out research projects on various environmental and resource management aspects from geothermal developments. This poses the biggest barrier for both regulatory bodies and project developers in the implementation of shared actions and continuous research to address technical and scientific solutions to different issues in the sector.

9 Conclusions

The method used to constrain the gas concentration in the geothermal fluid and the emissions from the power plant can be used as an alternative approach in cases where no reference data is available. The H_2S emissions from San Jacinto-Tizate power plant when it operates at full load for a whole year were estimated as 1436.2 tons/year. The same approach could be later used for planning purposes prior to project development in certain areas.

The results from AERMOD modeling for a whole year when the San Jacinto-Tizate power plant operated at full load (72 MW) shows that H_2S concentration at ground level can exceed the WHO ambient air guideline (150 $\mu g/m^3$ averaged over 24 h) in the immediate vicinity of the power plant (within 1 km W), but not in populated places and surrounding villages. The occupational exposure limits for H_2S in the working environment are not exceeded.

When comparing AERMOD predictions with measured H_2S concentrations during three different periods, the model underestimated the measured values in most of the monitoring points, except for two points that were greatly overestimated to the north of the power plant. The discrepancy can be associated to factors like the source input data used for modeling and the characteristics of the location of the control points, as well as the specific operation conditions of the power plant when the measurements are done and the influence of H_2S natural sources in the reported measured concentration.

Reporting the power plant operation conditions along with individual H_2S measurements could be used to analyze the variability of both measured and predicted concentrations depending on the weather conditions at a given time. A better analysis of correlation between the model predictions and measured concentrations could be done and additional sources for discrepancies in the results could be identified.

The spatial distribution of the plume was identified predominantly to the W, WNW and WSW of the power plant for the majority of the modeled periods. The air quality trend in case of future expansion of the power plant could be easily identified based on the modeling results, as well as the extension of the new impacted area. The most important weather conditions affecting the modeling results are the wind speed and direction along with the atmospheric stability during different hours of the day.

The modeling could be refined based on reliable data from the San Jacinto-Tizate Power plant. For this, the chemical composition of the steam as well as operational parameters from the cooling towers where the H_2S is emitted to the atmosphere is needed.

The results from AERMOD modeling provide useful information to analyze the spatial distribution and the extent of the plume during a given period; however the predicted H_2S concentration at specific locations should be considered indicative rather than accurate predictions of ground level concentrations. The modeling results however can assist policy

makers and project developers to review and propose improvements to the air quality monitoring plans as well as mitigating measures if needed.

The weather station installed in the project site by PENSA provides substantial data for air quality modeling. Nevertheless the installation of additional instruments to measure clouds and solar radiation at the site is recommended in order to provide a complete database of meteorological parameters.

The installation of a continuous monitoring station for H_2S at the project site is highly recommended to document the changes in air quality in real time. Until this measure is not implemented, the monitoring plan should be improved by increasing the duration and frequency of the monitoring periods. Air quality monitoring reports should also be upgraded by including hourly measurements in addition to averaged concentrations reported for comparison with air quality guidelines.

References

ACGIH. 2009. Threshold limit values (TLV) for chemical substance and physical agents and biological exposure indices (BES). Cincinnati, OH,: ACGIH.

AIHA. 1991. Emergency Response Planning Guideline for Hydrogen Sulfide. : American Industrial Hygiene Association.

Arnorsson, S. and Stefansson, A. 1999. Assessment of feldspar solubility constants in water in the range of 0 degrees to 350 degrees C at vapor saturation pressures. *American Journal of Science, 299*(3), 173-209. doi: 10.2475/ajs.299.3.173

Arnórsson, S.,Björnsson, S.,Muna, Z. W. and Bwire-Ojiambo, S. 1990. The use of gas chemistry to evaluate boiling processes and initial steam fractions in geothermal reservoirs with an example from the olkaria field, Kenya. *Geothermics, 19*(6), 497–514. doi: http://dx.doi.org/10.1016/0375-6505(90)90002-S

Arnórsson, S.,Fridriksson, T. and Gunnarsson, I. 1998. Gas Chemistry of the Krafla Geothermal field, Iceland. In G. B. Arehart and J. R. Hulston (Eds.), Water Rock Interaction (pp. 613-616). Rotterdam, Balkema.

Arnórsson, S. and Gunnlaugsson, E. 1985. New gas geothermometers for geothermal exploration-calibration and application. *Geochimica et Cosmochimica Acta, 49*(6), 1307–1325. doi: http://dx.doi.org/10.1016/0016-7037(85)90283-2

Arnórsson, S.,Gunnlaugsson, E. and Svavarsson, H. 1983. The chemistry of geothermal waters in Iceland. II. Mineral equilibria and independent variables controlling water compositions. *Geochimica et Cosmochimica Acta, 47*(3), 547–566. doi: http://dx.doi.org/10.1016/0016-7037(83)90277-6

Atkinson, D. and Lee, R. F. 1992. Procedures for substituting values for missing NWS meteorological data for use in regulatory air quality models.

Ármannsson, H.,Gíslason, G. and Hauksson, T. 1982. Magmatic gases in well fluids aid the mapping of the flow pattern in a geothermal system. *Geochimica et Cosmochimica Acta, 46*(2), 167–177. doi: http://dx.doi.org/10.1016/0016-7037(82)90244-7

Bacci, E.,Gaggi, C.,Lanzillotti, E.,Ferrozzi, S. and Valli, L. 2000. Geothermal power plants at Mt. Amiata (Tuscany-Italy): mercury and hydrogen sulphide deposition revealed by vegetation. *Chemosphere, 40*(8), 907-911.

Bates, M. N.,Garrett, N.,Crane, J. and Balmes, J. R. 2013. Associations of ambient hydrogen sulfide exposure with self-reported asthma and asthma symptoms. *Environ Res, 122*, 81-87. doi: 10.1016/j.envres.2013.02.002

Bates, M. N.,Garrett, N. and Shoemack, P. 2002. Investigation of health effects of hydrogen sulfide from a geothermal source. *Archives of Environmental Health: An International Journal, 57*(5), 405-411. doi: 10.1080/00039890209601428

Bird, D. K.,Schiffman, P.,Elders, W. A.,Williams, A. E. and McDowell, S. D. 1984. Calc-silicate mineralization in active geothermal systems. *Economic Geology, 79*(4), 671-695. doi: 10.2113/gsecongeo.79.4.671

Bird, D. K. and Spieler, A. R. 2004. Epidote in Geothermal Systems. *Reviews in Mineralogy and Geochemistry, 56*(1), 235-300. doi: 10.2138/gsrmg.56.1.235

Bloomfield, K.,Moore, J. and Neilson, R. 2003. Geothermal energy reduces greenhouse gases. *GRC Bulletin, Climate Change Research, March/April 2003,* 77-79.

BMacZero. 2012. Gaussian plume: Wikimedia Commons, the free media repository.

Browne, P. R. L. 1978. Hydrothermal Alteration in Active Geothermal Fields. *Annual Review of Earth and Planetary Sciences, 6*, 229-250. doi: DOI 10.1146/annurev.ea.06.050178.001305

Carlsen, H. K.,Zoëga, H.,Valdimarsdóttir, U.,Gíslason, T. and Hrafnkelsson, B. 2012. Hydrogen sulfide and particle matter levels associated with increased dispensing of anti-asthma drugs in Iceland's capital. *Environmental Research, 113*(0), 33-39. doi: http://dx.doi.org/10.1016/j.envres.2011.10.010

Chow-Pineda, I. 2007. Gaussian modelling of the dispersion of hydrogen sulphide from Hellisheidi power plant, Iceland *Geothermal training in Iceland* (pp. 55-78). Reykjavík, Iceland: UNU-GTP. Reports 2007, 5.

Cimorelli, A. J.,Perry1, S. G.,Venkatram, A.,Weil, J. C.,Paine, R. J.,Wilson, R. B.,Lee, R. F.,Peters, W. D.,Brode, R. W. and Paumier, J., O. 2004. AERMOD: description of model formulation: U.S. Environmental Protection Agency.

CNE. 2001. Nicaragua geothermal master plan (Vol. I): Report prepared by GeothermEx.

Collins, J. and Lewis, D. 2000. Hydrogen sulfide: evaluation of current california air quality standards with respect to protection of children: Report prepared for California Air Resources Board, California Office of Environmental Health Hazard Assessment.

D´Amore, F. and Panichi, C. 1980. Evaluation of deep temperatures in hydrothermal systems by a new gas geothermometer. *Geochimica et Cosmochimica Acta, 44*(3), 549–556. doi: http://dx.doi.org/10.1016/0016-7037(80)90051-4

D´Amore, F. and Truesdell, A. H. 1985. Calculation of geothermal reservoir temperatures and steam fractions from gas compositions. *Geotherm. Res. Counc. Trans., 9*, 305-310.

D'Alessandro, W. 2006. Gas hazard: an often neglected natural risk in volcanic areas. In J. F. Martin-Duque, C. A. Brebbia, D. E. Emmanouloudis and U. Mander (Eds.), *Geo-environment and landscape evolution II* (pp. 369-378). South Hapmpton: WIT Press.

Dickson, M. H. and Fanelli, M. 2003. *Geothermal energy: utilization and technology*. Paris: United Nations Educational, Scientific and Cultural Organization.

Durand, M. and Wilson, J. G. 2006. Spatial analysis of respiratory disease on an urbanized geothermal field. *Environmental Research, 101*(2), 238-245. doi: http://dx.doi.org/10.1016/j.envres.2005.08.006

Establishing a third list of indicative occupational exposure limit values in implementation of Council Directive 98/24/EC and amending Commission Directive 2000/39/EC, Commission directive 2009/161/EU C.F.R. 2009.

Freedman, A. J. E.,Bird, D. K.,Arnórsson, S.,Fridriksson, T.,Elders, W. A. and Fridleifsson, G. Ó. 2009. Hydrothermal minerals record CO_2 partial pressures in the Reykjanes geothermal system, Iceland. *American Journal of Science, 309*(9), 788-833. doi: 10.2475/09.2009.02

Giggenbach, W. F. 1980. Geothermal Gas Equilibria. *Geochimica Et Cosmochimica Acta, 44*(12), 2021-2032. doi: Doi 10.1016/0016-7037(80)90200-8

Giggenbach, W. F. 1981. Geothermal Mineral Equilibria. *Geochimica Et Cosmochimica Acta, 45*(3), 393-410. doi: Doi 10.1016/0016-7037(81)90248-9

Giggenbach, W. F. 1992. Isotopic Shifts in Waters from Geothermal and Volcanic Systems Along Convergent Plate Boundaries and Their Origin. *Earth and Planetary Science Letters, 113*(4), 495-510. doi: Doi 10.1016/0012-821x(92)90127-H

Gill, J. B. 1981. *Orogenic andesites and plate tectonics*. New York: Springer-Verlag.

Giunta, G. and Orioli, S. 2011. *The Caribbean Plate evolution: trying to resolve a very complicated tectonic puzzle*. New Frontiers in Tectonic Research - General Problems, Sedimentary Basins and Island Arcs, Prof. Evgenii Sharkov (Ed.), ISBN: 978-953-307-595-2, InTech, DOI: 10.5772/18723.

Gudmundsson, B. T. and Arnorsson, S. 2002. Geochemical monitoring of the Krafla and Námafjall geothermal areas, N-Iceland. *Geothermics, 31*(2), 195-243. doi: http://dx.doi.org/10.1016/S0375-6505(01)00022-0

Gudmundsson, B. T. and Arnorsson, S. 2005. Secondary mineral-fluid equilibria in the Krafla and Namafjall geothermal systems, Iceland. *Applied Geochemistry, 20*(9), 1607-1625. doi: DOI 10.1016/j.apgeochem.2005.04.020

Gunnarsson, I.,Aradóttir, E. S.,Sigfússon, B.,Gunnlaugsson, E. and Júlíusson, B. 2013. Geothermal gas emission from Hellisheiði and Nesjavellir power plants, Iceland. *GRC Transactions, 37,* 785-789.

Gunnarsson , I.,Aradóttir, E. S.,Sigfússon , B.,Gunnlaugsson, E. and Júlíusson , B. 2013. Geothermal Gas Emission From Hellisheiði and Nesjavellir Power Plants, Iceland. *GRC Transactions, 37*.

Heaney, C. D.,Wing, S.,Campbell, R. L.,Caldwell, D.,Hopkins, B.,Richardson, D. and Yeatts, K. 2011. Relation between malodor, ambient hydrogen sulfide, and health in a community bordering a landfill. *Environ Res, 111*(6), 847-852. doi: 10.1016/j.envres.2011.05.021

Holm, A.,Jennejohn, D. and Blodgett, L. 2012. Geothermal energy and greenhouse gas emissions (pp. 14). Washington DC: Geothermal Energy Association.

Hunt, T. 2000. Five lectures on environmental effects on geothermal energy utilization. In UNU-GTP (Ed.), (Vol. Reports 2000, pp. 1-109). Reykjavık, Iceland.

IDB. 2010. San Jacinto-Tizate geothermal power project (NI-L1057). *Environmental and Social Management Report* Inter American Development Bank.

Idriss, A.,Foster, K. R.,Yee, D.,Palczynski, R.,Dixon, E.,Jackson, W. and Kinneburgh, C. 2004. Assessment report on reduced sulphur compounds for developing ambient air quality objectives: Report prepared for Alberta Environment.

Ingimunarsson, A. and Thorhallsson, S. 2012. *Evaluation of technical feasibility of the geothermal power plant in San Jacinto-Tizate, Nicaragua*. ISOR-2012/060. Report prepared for ICEIDA. Unpublished report.

IUCN. 2012. Gobal protected areas programme. Protected Areas Category V. Retrieved May 15, 2014, from http://www.iucn.org/about/work/programmes/gpap_home/gpap_quality/gpap_pacategories/gpap_category5/

IVHHN. 2014. Hydrogen sulphide (H_2S). *Volcanic Gases and Aerosols Index.* Retrieved 05.05, 2014, from http://www.ivhhn.org/index.php?option=com_content&view=article&id=83

Jappinen, P.,Vilkka, V.,Marttila, O. and Haahtela, T. 1990. Exposure to hydrogen sulphide and respiratory function. . *Br. J. Ind. Med, 47*(12), 824-828.

Johnson, J. W.,Oelkers, E. H. and Helgeson, H. C. 1992. SUPCRT92: A software package for calculating the standard molal thermodynamic properties of minerals, gases, aqueous species, and reactions from 1 to 5000 bar and 0 to 1000°C. *Computers & Geosciences, 18*(7), 899-947. doi: http://dx.doi.org/10.1016/0098-3004(92)90029-Q

Karingithi, C. W.,Arnórsson, S. and Grönvold, K. 2010. Processes controlling aquifer fluid compositions in the Olkaria geothermal system, Kenya. *Journal of Volcanology*

and Geothermal Research, 196(1–2), 57-76. doi: http://dx.doi.org/10.1016/j.jvolgeores.2010.07.008

Khoirunissa, I. 2011. Hydrogen sulfide dispersion for Hellisheidi and Nesjavellir geothermal power plants in Iceland using AERMOD. *Geothermal training in Iceland* (pp. 249-280). Reykjavík, Iceland: UNU-GTP. Reports 2011, 14.

Kilburn, K. H. and Warshaw, R. H. 1995. Hydrogen sulfide and reduced-sulfur gases adversely affect neurophysiological functions. *Toxicol. Ind. Health, 11*, 185-197.

Kristmannsdóttir, H.,Sigurgeirsson, M.,Ármannsson, H.,Hjartarson, H. and Ólafsson, M. 2000. Sulfur gas emissions from geothermal power plants in Iceland. *Geothermics, 29*(4-5), 525-538. doi: http://dx.doi.org/10.1016/S0375-6505(00)00020-1

Li, Z. G. 2013. Hydrogen sulfide: A multifunctional gaseous molecule in plants. *Russian Journal of Plant Physiology, 60*(6), 733-740. doi: 10.1134/S1021443713060058

Arizona Instrument LLC. 2014. Jerome 631-X hydrogen sulfide analyzer. Retrieved 20/04, 2014, from http://www.azic.com/products_jerome_631.aspx

Martin, D. O. 1976. Comment on change of concentration standard deviations with distance. *Journal of the Air Pollution Control Association, 26*(2), 145-146.

McBirney, A. R. and Williams, H. 1965. *Volcanic History of Nicaragua*: University of California Press.

Morris, P. and Therivel, R. 1995. *Methods of environmental impact assessment*. Vancouver: UBC Press.

Nagl, G. J. 1999 Controlling H_2S emissions in geothermal power plants. *Bulletin d'Hydrogéologie* (pp. 393-402): Centre d'Hydrogeologie, Universite de Neuchatel.

Nehring, N. L. and Damore, F. 1984. Gas Chemistry and Thermometry of the Cerro-Prieto, Mexico, Geothermal-Field. *Geothermics, 13*(1-2), 75-89. doi: Doi 10.1016/0375-6505(84)90008-7

Nevers, N. 2000. *Air pollution control engineering* (2nd ed.). Boston: McGraw-Hill.

NIOSH. 2005. Hydrogen sulphide. Retrieved from www.cdc.gov/niosh/npg/npgd0337.html

Ogryzlo, C. T. and Randle, J. B. 2005. *Financing the San Jacinto-Tizate geothermal project in Nicaragua*. Paper presented at the World Geothermal Congress, Antalya, Turkey. http://www.geothermal-energy.org/pdf/IGAstandard/WGC/2005/0409.pdf

OSHA. 2006. Toxic and hazardous substances, Standards 29 CFR, Table Z-2. *Occupational Safety and Health Standards.* Retrieved from https://www.osha.gov/pls/oshaweb/owadisp.show_document?p_id=9993&p_table=STANDARDS

Ostapenko, S. V.,Spektor, S. V. and Netesov, Y. P. 1998. San Jacinto-Tizate geothermal field, Nicaragua: Exploration and conceptual model. *Geothermics, 27*(3), 361-378. doi: http://dx.doi.org/10.1016/S0375-6505(98)00007-8

Ólafsdóttir, S. 2007. *Modeling of hydrogen sulfide concentration in Reykjavik City due to emissions from geothermal power plants.* University of Iceland, Reykjavík. Retrieved from http://www.hi.is/umhverfis_og_byggingarverkfraedideild/meistaraverkefni_snjolaug_olafsdottir

Ólafsdóttir, S.,Gardarsson, S. M. and Andradottir, H. O. 2014. Spatial distribution of hydrogen sulfide from two geothermal power plants in complex terrain. *Atmospheric Environment, 82*(0), 60-70. doi: http://dx.doi.org/10.1016/j.atmosenv.2013.10.013

PENSA. 2008. Estudio de impacto ambiental (EIA). Proyecto reconversión tecnológica en San Jacinto-Tizate para la generación de 72 MW de energía eléctrica: Reporte preparado por CABAL S.A., in Spanish.

PENSA. 2012. *Informe de gestión ambiental 2012*. Unpublished report. Polaris Energy Nicaragua S.A., in Spanish.

PENSA. 2013. *Informe de gestión ambiental 2013*. Unpublished report. Polaris Energy Nicaragua S.A., in Spanish.

Quintero-Roman, R. 2010. Borehole Geology of Well SJ9-2, San Jacinto-Tizate geothermal field, NW-Nicaragua *Geothermal training in Iceland* (pp. 563-588). Reykjavík, Iceland: UNU-GTP. Reports 2010, 27.

Ram Power, C. 2013. Operational Update. San Jacinto-Tizate Remediation Drilling Program. Retrieved from http://ram-power.com/sites/default/files/assets/news-documents/Corporate%20Update%20PR%20FINAL_0.pdf

Reed, B. R.,Crane, J.,Garrett, N.,Woods, D. L. and Bates, M. N. 2014. Chronic ambient hydrogen sulfide exposure and cognitive function. *Neurotoxicol Teratol, 42*, 68-76. doi: 10.1016/j.ntt.2014.02.002

Schinasi, L.,Horton, R. A.,Guidry, V. T.,Wing, S.,Marshall, S. W. and Morland, K. B. 2011. Air pollution, lung function, and physical symptoms in communities near concentrated Swine feeding operations. *Epidemiology, 22*(2), 208-215. doi: 10.1097/EDE.0b013e3182093c8b

Schulman, L. L. and Scire, J. S. 1980. Buoyant line and point source (BLP) dispersion model user's guide: Environmental Research & Technology, Inc.

Seangkiatiyuth, K.,Surapipith, V.,Tantrakarnapa, K. and Lothongkum, A. W. 2011. Application of the AERMOD modeling system for environmental impact assessment of NO2 emissions from a cement complex. *Journal of Environmental Sciences, 23*(6), 931-940. doi: http://dx.doi.org/10.1016/S1001-0742(10)60499-8

SKM. 2008. *Drilling completion report on well SJ9-2*. Unpublished report for Polaris Energy Nicaragua S.A. Sinclair Knight Merz.

Spektor, S. V. 1994. *Report on geologic map of San Jacinto-Tizate geothermal field, Nicaragua*. Intergeoterm, S.A., unpublished report.

Stefansson, A. and Arnorsson, S. 2000. Feldspar saturation state in natural waters. *Geochimica Et Cosmochimica Acta, 64*(15), 2567-2584. doi: Doi 10.1016/S0016-7037(00)00392-6

R Core Team. 2013. R: A language and environment for statistical computing. Vienna, Austria: R Foundation for Statistical Computing. Retrieved from http://www.R-project.org/

Thorsteinsson, T.,Hackenbruch, J.,Sveinbjörnsson, E. and Jóhannsson, T. 2013. Statistical assessment and modeling ofthe effects of weather conditions on H_2S plume dispersal from Icelandic geothermal power plants. *Geothermics, 45*, 31–40.

Turner, D. B. 1994. *Workbook of atmospheric dispersion estimates: an introduction to dispersion modeling* (2nd ed.). Boca Raton: Lewis Publishers.

USEPA. 1999. Integrated Risk Information System (IRIS) database. Hydrogen sulfide (CASRN 7783-06-4). Reference concentration for chronic inhalation exposure (RfC). Retrieved from http://www.epa.gov/iris/subst/0061.htm

USEPA. 2003. Toxicological review of hydrogen sulfide (CAS No. 7783-06-4): In Support of Summary Information on the Integrated Risk Information System (IRIS). U.S. Environmental Protection Agency.

USEPA. 2005 Basic air pollution meteorology. Self Instructional Manual. *APTI Course SI: 409 (Rev. April, 2005)*

Webster, J. G. 1995. Chemical impacts of geothermal development. In K. L. Brown (Ed.), *Environmental aspects of geothermal development* (pp. 79-95). Pisa, Italy: World Geothermal Congress 1995, IGA pre-congress course.

Weinberg, R. F. 1992. Neotectonic development of western Nicaragua. *Tectonics, 11*(5), 1010-1017. doi: 10.1029/92TC00859

White, P.,Lawless, J.,Ussher, G. and Smith, A. 2008. *Recent results from the San Jacinto-Tizate geothermal field, Nicaragua.* Paper presented at the New Zealand Geothermal Workshop.

WHO. 2000. Air quality guidelines for Europe (Second ed.). Copenhagen, Denmark: WHO Regional Office for Europe.

WHO. 2003. Hydrogen sulfide: human health aspects. *Concise International Chemical Assessment* (pp.). Geneva: World Health Organization.

Zannetti, P. 1990. *Air pollution modeling: theories, computational methods, and available software*. Southampton; Boston New York: Computational Mechanics Publications; Van Nostrand Reinhold.

Zúñiga, A. 2003. Geothermal Nicaragua. *GRC Bulletin, International Geothermal development,* 163-166.

Appendix A

Calculated equilibrium constants as a function of temperature for mineral assemblage reactions considered in this study.

Table A-1. Equilibrium constants for reactions, correspondent activity and H_2S concentration in deep liquid and steam at 10 bar-a.

Temperature C	Reaction	LOG K	LOG (H_2S)	a(H_2S) = m(H_2S)	H_2S (ppm) Deep liquid	H_2S (ppm) Steam
200	a	-3.8312	-3.7916	1.62E-04	5.49	123.37
210	a	-3.6407	-3.6011	2.51E-04	8.52	127.08
220	a	-3.4553	-3.4157	3.84E-04	13.05	145.32
230	a	-3.2747	-3.2350	5.82E-04	19.79	175.21
240	a	-3.0982	-3.0585	8.74E-04	29.71	217.78
250	a	-2.9254	-2.8858	1.30E-03	44.23	275.85
260	a	-2.7559	-2.7163	1.92E-03	65.34	353.71
270	a	-2.5893	-2.5497	2.82E-03	95.89	457.31
275	a	-2.5070	-2.4674	3.41E-03	115.91	521.17
280	a	-2.4252	-2.3856	4.12E-03	139.92	594.64
290	a	-2.2633	-2.2237	5.97E-03	203.14	776.34
300	a	-2.1032	-2.0635	8.64E-03	293.72	1016.47
200	b	-3.8600	-3.8600	1.38E-04	4.6936	105.39
210	b	-3.6912	-3.6912	2.04E-04	6.9226	103.26
220	b	-3.5269	-3.5269	2.97E-04	10.1050	112.49
230	b	-3.3667	-3.3667	4.30E-04	14.6149	129.39
240	b	-3.2100	-3.2100	6.17E-04	20.9648	153.66
250	b	-3.0564	-3.0564	8.78E-04	29.8577	186.21
260	b	-2.9056	-2.9056	1.24E-03	42.2564	228.74
270	b	-2.7571	-2.7571	1.75E-03	59.4815	283.66
275	b	-2.6836	-2.6836	2.07E-03	70.4465	316.75
280	b	-2.6106	-2.6106	2.45E-03	83.3459	354.22
290	b	-2.4657	-2.4657	3.42E-03	116.3430	444.62
300	b	-2.3222	-2.3222	4.76E-03	161.9094	560.32
200	c	-49.416	-4.4924	3.22E-05	1.0942	24.57
210	c	-47.259	-4.2963	5.06E-05	1.7187	25.64
220	c	-45.172	-4.1065	7.82E-05	2.6603	29.61
230	c	-43.15	-3.9227	1.19E-04	4.0621	35.96
240	c	-41.19	-3.7445	1.80E-04	6.1226	44.88
250	c	-39.288	-3.5716	2.68E-04	9.1168	56.86

Temperature C	Reaction	LOG K	LOG (H_2S)	a(H_2S) = m(H_2S)	H_2S (ppm) Deep liquid	H_2S (ppm) Steam
260	c	-37.44	-3.4036	3.95E-04	13.4228	72.66
270	c	-35.642	-3.2402	5.75E-04	19.5568	93.26
275	c	-34.761	-3.1601	6.92E-04	23.5173	105.74
280	c	-33.891	-3.0810	8.30E-04	28.2149	119.91
290	c	-32.183	-2.9257	1.19E-03	40.3415	154.17
300	c	-30.512	-2.7738	1.68E-03	57.2349	198.07
200	d	-103.347	-4.6518	2.23E-05	0.7580	17.02
210	d	-98.783	-4.4443	3.59E-05	1.2222	18.23
220	d	-94.368	-4.2437	5.71E-05	1.9401	21.60
230	d	-90.092	-4.0493	8.93E-05	3.0352	26.87
240	d	-85.947	-3.8609	1.38E-04	4.6838	34.33
250	d	-81.926	-3.6781	2.10E-04	7.1346	44.50
260	d	-78.02	-3.5006	3.16E-04	10.7378	58.12
270	d	-74.221	-3.3279	4.70E-04	15.9808	76.21
275	d	-72.36	-3.2433	5.71E-04	19.4173	87.31
280	d	-70.522	-3.1597	6.92E-04	23.5361	100.03
290	d	-66.914	-2.9957	1.01E-03	34.3348	131.22
300	d	-63.387	-2.8354	1.46E-03	49.6652	171.88